Superconducting Transmon Qubit; Control and Characterisation

Dissertation submitted by

Kaustav Ghosh

University Enroll. No : 002220802007
Registration No : 165379 of 22-23

Supervisor : **Prof. Bhupendra Nath Dev**
Centre for Quantum Engineering, Research and Education (CQuERE)
TCG CREST, Kolkata

In partial fulfillment of the
M.Sc. degree in Instrumentation Science

Department of Instrumentation Science
Jadavpur University, Kolkata 700032

June, 2024

Certificate

This hereby affirms that the project entitled "Superconducting Transmon Qubit; Control and Characterisation" submitted by Mr. Kaustav Ghosh, Roll No: 002220802007, Registration No: 165379 of 22-23 in partial fulfilment of the degree of Master of Science in Instrumentation Science of Jadavpur University is an authentic work carried out under Prof. Bhupendra Nath Dev's supervision and guidance. The matter embodied in this project has not been submitted to any other University/Institute for the award of Degree or Diploma.

Prof. Bhupendra Nath Dev

Self Declaration

I, Mr. Kaustav Ghosh, a bonafied student at the Department of Instrumentation Science, Jadavpur University hereby declare that this thesis presented for the degree of M.Sc. in Instrumentation Science from the department, has been composed solely by myself and that it has not been submitted, in whole or in part, in any previous application for a degree or diploma.

I confirm that this thesis is composed of my original work, and contains no material previously published or written by another person except where due references has been made in the text.

The content of my thesis is the result of work I have carried out with the Superconducting Qubit team at CQuERE, TCG CREST since the commencement of the fourth semester at the university. The experimental work done in this thesis is almost entirely my own work with the collaborative contributions from the team under the guidance of Prof. Bhupendra Nath Dev and Dr. Snehal Mandal have been indicated clearly and acknowledged. Due references have been provided on all supporting litterateurs and resources.

Kaustav Ghosh
kaustavghosh@hotmail.com

"And God called the light Day, and the darkness he called Night. And the evening and the morning were the first day." **- Genesis**

Dedicated to

My Parents,
and the cat who is still furious for it was kept in a box

Acknowledgement

To begin with, it is an absolute honour to be able to express my heartfelt gratitude to Prof. Bhupendra Nath Dev, for providing me with this incredible opportunity to undertake and successfully complete my master's project under his expert supervision. His invaluable insights along with his ever smiling and approachable nature, have been instrumental in shaping the direction and outcome of this project. I consider myself nothing but blessed to have had the privilege of working with him.

I am deeply indebted to Mr. Sudhindu Bikash Mandal for introducing me to the fascinating field of Quantum Computation during the numerous discussions I was fortunate enough to have. His unwavering support and encouragement have played a significant role in nurturing my interest in this subject.

I would also like to extend my gratefulness to my mentor, Dr. Snehal Mandal. During my time at CQuERE(TCG CREST), his assistance throughout has been indispensable in the completion of my project. I am sincerely thankful for the patience and kindness he has consistently shown me throughout this journey.

My duration at CQuERE would have never been as enriching as it is without Biplab Biswas, Ayan Kumar Ghosh, Souvik Chatterjee, Dean Poulos and the hours long exchanges of thought we shared. While I move forward in my journey, I wish to extend my best wishes to them for their future endeavors. I am in loss of word with the lasting memories and friendships I have made during my time at CQuERE.

As I believe, we not only are standing on the shoulders of giants, but our fellows as well and as it is destined to become quite an audacious adventure if one tries to take names of each and everyone who has and had helped along the way, I would rather express the fact from the bottom of my heart that I could be no less than confoundingly blessed.

Abstract

Superconducting qubits are on the cutting edge of quantum processor research and development, requiring amplitude and phase-modulated microwave frequency pulses to control and monitor. This dissertation focuses on the control and characterization of a superconducting qubit. It starts with theoretical understanding and advances to experimental setups and experiments, followed by result analysis and characterization. The utmost aspiration for this project is to institute a quantum processor and peripheral system that is prepared and optimized for computing activities. In the studies mentioned, the experiments have been conducted using a single superconducting transmon qubit connected to a 3D cavity system.

In this dissertation, we will begin with discussing about the basic realisations of a superconducting qubit and it's interaction with the environment which is essential for probing the qubit using circuit quantum electrodynamics, followed by an idea of the control environment, readout and the qubit dynamics in chapter 2. The experimental arrangements needed and used are talked about in chapter 3. We then proceed on to the experimental methodology for qubit manipulation and characterisation in chapter 4. In Chapter 5,results are reported and analysed. Concluding the research, parting remarks are left in Chapter 6.

Key words: *Quantum computer, Qubit, Transmon, Microwave, Resonator*

Contents

Chapter 1

Introduction

1.1 Quantum Computer: Why and What?

Although classical computers have reached a long way since their inception, as the years pass, the problems to be tackled by them are getting harder and more intractable. Feynman, like the visionary, predicted the need for computers, which, rather than using classical principles, harnesses quantum concepts. In his key speech, Feynman famously remarked, *"Nature isn't classical, dammit, and if you want to make a simulation of Nature, you'd better make it quantum mechanical, and by golly it's a wonderful problem because it doesn't look so easy"*[1]. Bringing to life Feynman's vision emerges as a monumental endeavor for science and technology in the 21st century, although remarkable strides have been made in this regard , a scalable quantum computer to simulate complex quantum systems still remains a challenge.

1.2 Qubits

Like the classical computer bit, the qubit, or quantum bit, is the soul of a quantum computer and the basic unit of quantum information. According to the laws of quantum mechanics, qubits can exist simultaneously in a superposition of both high and low states. In contrast, classical bits can only be in one of two states, which are either 0 or 1. This shows that, compared to a classical bit, a qubit can represent and process much more information, as the efficiency of a computing instrument is measured against the space, energy, and time used. Qubits can also experience entanglement, where the states of two qubits become entangled and dependent on each other. This allows qubits to be connected in complex ways, leading to advancements in quantum information science through the development of robust algorithms and protocols.

In practical implementations, qubits are often realized using various quantum mechanical systems such as;

- Trapped ion
- Superconducting Qubit
- Spin Qubit
- Photonic Qubit
- Defect based Qubits- Nitrogen vacancy(NV) in diamond

These systems allow for precise control and manipulation of individual qubits and their quantum state, developing quantum computers and other quantum technologies with the potential to revolutionize various fields, including cryptography, chemistry, information science, optimization, and materials science.

However, all these implementations have been plagued by the loss of quantum information with time named decoherence, which arises from noise introduced through the interplay between the quantum systems and their environment. Practical quantum computation can only be achieved when decoherence times are pushed further, gates made faster, and the number of qubits scaled higher. The field confronts challenges and unresolved issues, addressing which requires innovative engineering approaches and theoretical advancements. Techniques like error correction codes and improved qubit designs are being explored to mitigate decoherence effects and enhance the performance of quantum computers. rendering it a dynamic and engaging area of exploration.

1.2.1 Superconducting Qubits

Superconductor-based qubits, due to their ratio of gate operation to coherence time, are one of the front-runners in the endeavor to fabricate a tangible quantum computer. Superconducting LC oscillator circuits(Figure1.1) with their dissipation free environment can be used to realize superconducting qubits. Superconductivity, a macroscopic quantum phenomenon which occurs when cooper pairs or paired electrons condense into a single bosonic state. With a superconductor, resonant electrical circuits with inductors and capacitors can readily be fabricated. The energy of a superconducting LC oscillator can be written as;

$$H = \frac{Q^2}{2C} + \frac{\Phi^2}{2L} \tag{1.1}$$

where charge in the capacitor is Q and Φ is the flux in the inductor. These are regarded as canonical momentum and position variables respectively.

$$\frac{\partial H}{\partial Q} = \frac{Q}{C} = V = -L\frac{\partial I}{\partial t} = -\dot{\Phi} \tag{1.2}$$

$$\frac{\partial H}{\partial \Phi} = \frac{\Phi}{L} = I = \dot{Q} \tag{1.3}$$

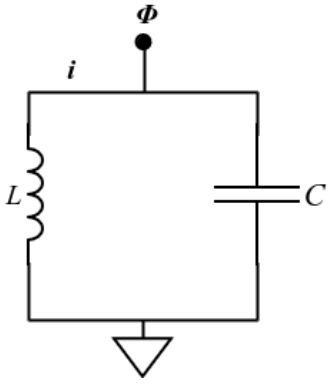

Figure 1.1: LC oscillator.

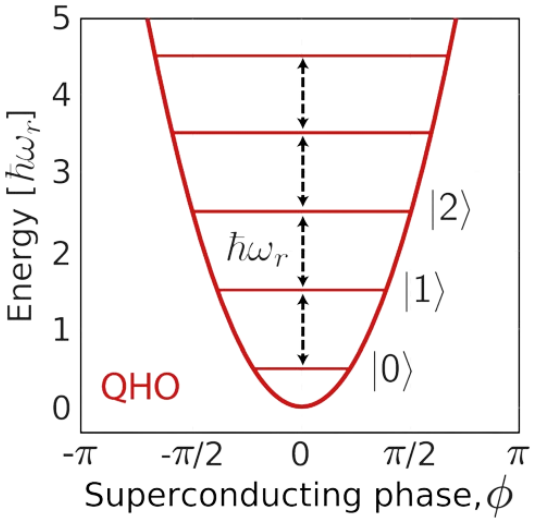

Figure 1.2: Quantum harmonic oscillator(QHO) energy level[2].

Further, we can extend the canonical variables to their quantum mechanical counterparts, $\hat{Q}$ and $\hat{\Phi}$ such that $[\hat{Q}, \hat{\Phi}] = -i\hbar$. The Hamiltonian now becomes quantized[2].

$$\hat{H} = \frac{\hat{Q}^2}{2C} + \frac{\hat{\Phi}^2}{2L} \tag{1.4}$$

In a superconducting circuit, if n is the number of cooper pair(reduced charge), $n = Q \,/\, 2e$ and reduced flux $\phi = 2\pi\Phi \,/\, \Phi_0$. Charging energy for adding each cooper pair $E_C = e^2 \,/\, 2C$ and the inductive energy is, $E_L = (\Phi_0 \,/\, 2\pi)^2 \,/\, L$ with $\Phi_0 = h \,/\, 2e$ being the superconducting magnetic flux quantum. The Hamiltonian is;

$$\hat{H} = 4E_C\hat{n}^2 + \frac{1}{2}E_L\hat{\phi}^2 \tag{1.5}$$

ϕ and n satisfies a commutation relation.

$$[\phi, n] = i \tag{1.6}$$

Hamiltonian in E.q.(1.5) is similar to that of a 1D quantum harmonic oscillator. This outcome can be expressed more succinctly in the context of the QHO Hamiltonian as;

$$H = \hbar\omega_r(a^\dagger a + \frac{1}{2}) \tag{1.7}$$

$a^\dagger$ and a is the creation and annihilation operator for a lone excitation of the resonator and denoted by $\omega_r = 1 \,/\, \left(\sqrt{LC}\right)$, is the resonance frequency of the system. The linear characteristics of QHO have a natural impediment towards its applications in processing quantum information with it's equidistant energy levels for once drive frequency tuned to ω_r(Figure1.2), there is nothing stopping the system to translate into any energy-level one at a time. Before using the system as a qubit, we must be able to construct a computational subspace with only two[1] energy

[1]Usually the lowest two

states where transitions can occur selectively, without seeping into other levels within the system. To mitigate this problem and to create a two level computational subspace, we have to add anharmonicity in such a way that transition frequency from $|0\rangle$ to $|1\rangle$ is significantly different for transition from $|1\rangle$ to $|2\rangle$.

Josephson junction and the introduction of anharmonicity

To introduce non-equidistant energy levels for the oscillator, Josephson junction, i.e., a superconductor to insulator to superconductor junction, is utilized as a non-linear inductor(Figure1.3). It enables us to utilize the oscillator's lowest two energy states as the qubit subspace. It confines any stimulation to the upper levels while probing the qubit with transition frequency. The relationships describing the current and potential across the junction are as follows;

$$I = I_c \sin\phi \tag{1.8}$$

$$\frac{d\phi}{dt} = \frac{2\pi V}{\Phi_0} \tag{1.9}$$

where ϕ is the phase difference between the two superconducting states, I_c is the critical current, V is voltage disparity spanning the junction, I serves as current and Φ_0 embodies the flux quantum. These two relations can be utilized to calculate the inductance for the junction;

$$L_J(\Phi) = \frac{\Phi_0}{2\pi I_c} \frac{1}{\cos(2\pi\Phi/\Phi_0)} \tag{1.10}$$

using E.q.(1.9) as $\phi(t) = \frac{2\pi}{\Phi_0}\int_{\infty}^{t} V(t')\,dt' = 2\pi\Phi(t)/\Phi_0$. As we can see, the Josephson inductance L_J is non-linear. To acquire the qubit Hamiltonian, it is essential for us to calculate the energy corresponding to Josephson Junction;

$$\begin{aligned} E &= \int V(t)I(t)\,dt \\ E &= \int \frac{d\Phi}{dt} I_c \sin\phi\,dt \\ &= -E_J \cos\left(2\pi\Phi/\Phi_0\right) \end{aligned} \tag{1.11}$$

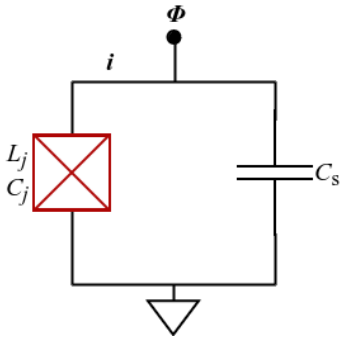

Figure 1.3: Nonlinear oscillator with Josephson Junction.

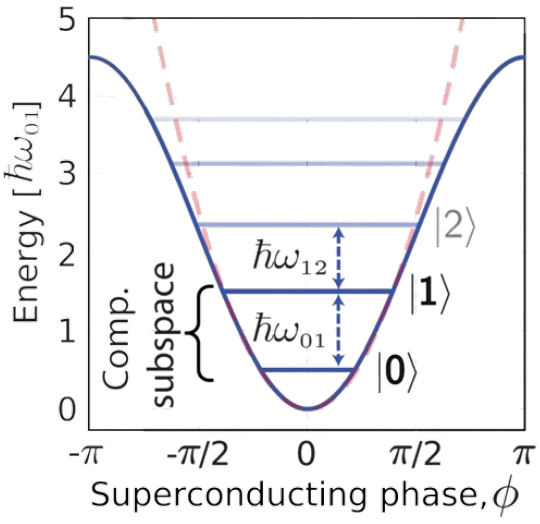

Figure 1.4: Quantum anharmonic oscillator(QAO) energy level using Josephson junction[2].

With $E_J = \frac{I_c \Phi_0}{2\pi}$, Hamiltonian for the qubit is expressed as;

$$\begin{aligned} \hat{H} &= \frac{\hat{Q}^2}{2C_\Sigma} - E_J \cos\left(2\pi\hat{\Phi}/\Phi_0\right) \\ &= 4E_C\hat{n}^2 - E_J \cos\hat{\phi} \end{aligned} \tag{1.12}$$

$C_\Sigma = C_j + C_s$which is the total capacitance and from E.q.(1.5), $\hat{n} = \hat{Q}\ /\ 2e$ and $E_C = e^2\ /\ 2C_\Sigma$ Here we will get different required frequency for different transition(Figure1.4) i.e. ω_{01} differing from ω_{12}. Thus with $|0\rangle$to $|1\rangle$ transition frequency tuned in, we confined the qubit within $|0\rangle$ and $|1\rangle$ states for using it in a computational system.

Transmon and the precise engineering of its Hamiltonian

This section covers the Transmon , a unique class of superconducting qubits. The qubit is connected to a drive line using capacitive coupling(Figure1.5). We use the drive to control the qubit states.

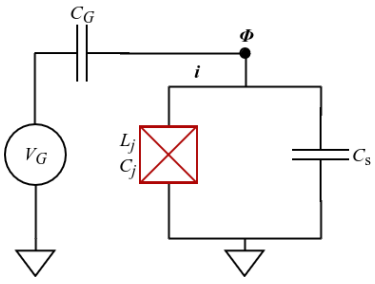

Figure 1.5: Circuit representation of a Transmon.

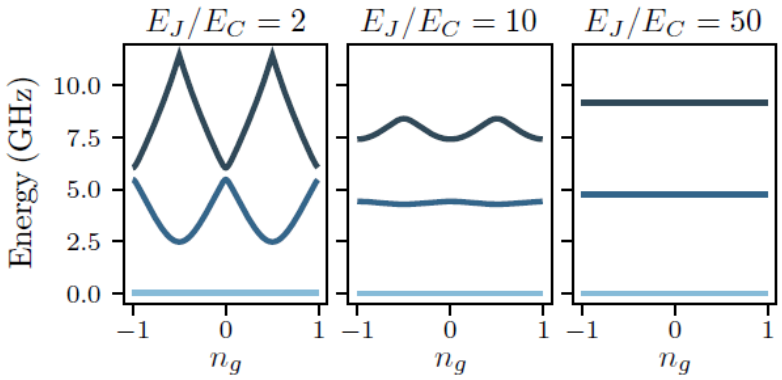

Figure 1.6: Energy difference (ω_j - ω_o) of first three energy levels with respect to offset charge and as functions of E_J / E_C [3].

After performing circuit quantization, the Hamiltonian becomes;

$$\begin{aligned}\hat{H} &= \frac{(\hat{Q}^2 - Q_g)}{2C_\Sigma} - E_J \cos\left(2\pi\hat{\Phi} \,/\, \Phi_0\right) \\ &= 4E_C(\hat{n}^2 - n_g) - E_J \cos\hat{\phi} \end{aligned} \tag{1.13}$$

The parameter Q_g accounts for any offset charge that may arise from drive voltage, or any unwanted charge in Transmon's environment. If we solve Schrodinger's equation for the Hamiltonian, first three energy levels as functions of E_J and E_C will look like as illustrated in figure(Figure1.6).

Interesting thing to notice here is, with increasing E_J / E_C ratio, energy levels gradually get insensitive to any offset charges. This is desirable, and we choose this because we wish to lessen the impact of undesired charges on the qubit. It is key to lay stress on the fact that, with the proper driving voltage, we can still manipulate the qubit states. All of these come at the expense of lessened anharmonicity. Thus, in the regime where E_J / E_C relatively high, transmon is a weak anharmonic oscillator.

1.3 Cavity Quantum Electrodynamics

A quantum measurement begins with entangling the quantum degree of freedom(DOF) of the qubit to an indicator variable. This is then followed by classically measuring the probe. Here, the qubit is in a state that is entangled with a pointer from a superconducting resonator. Circuit QED allows us to investigate the state of the qubit by inspecting the resonator instead of trying to have a firsthand engagement with it. As a result, optimizing readout performance entails increasing the signal-to-noise ratio(SNR) of the microwave probing signal supplied to the resonator while reducing undesirable back-actions on the qubit.

The discussion of the interaction between the quantum harmonic oscillator and the transmon can now proceed. Transmon qubits are inherently large and can be capacitively connected to microwave resonators with ease due to their huge capacitance (figure1.7), which results from the necessity of the shunt capacitor to have a small charging energy[1]. Solving Maxwell's wave equa-

[1] $E_C << E_J$

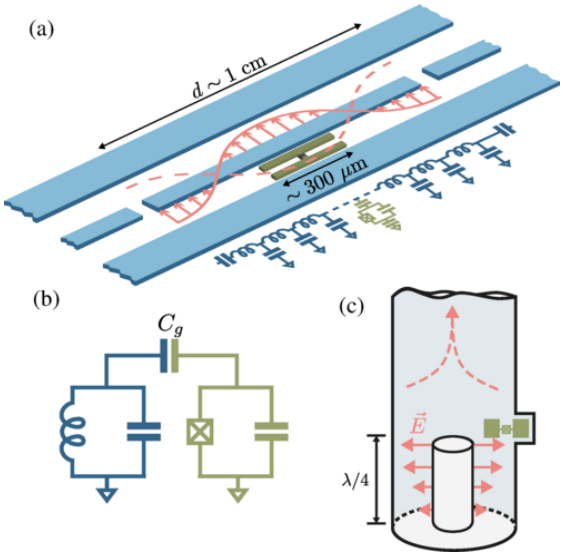

Figure 1.7: Schematic representation of a transmon qubit(green) coupled to (a) 1D transmission-line resonator[4]; (b) a lumped-element LC circuit; (c) a 3D coaxial cavity[3, 5].

tions within a cavity where the boundary conditions are defined yields specific correlations that should fulfill the wave vector k. Generally, the electro-magnetic (EM) field modes are referred to as being quantized. The qubit is placed in a 3D cavity where it experiences vacuum Rabi oscillations defined by cavity quantum electrodynamics and the Jaynes-Cummings model. We use this qubit-cavity/resonator engagement of the qubit with the surrounding cavity for performing qubit operations and read them out.

Considering a cylindrical cavity of length L housing the qubit at the center, with the qubit's dimensions being considerably smaller than that of the cavity or L, it is thus safe and reasonable for us to postulate that the qubit engages with the field at $L\ /\ 2$ [1]. The interaction is a dipole interaction with a Hamiltonian;

$$\hat{H}_{interaction} = \hat{d}.\hat{E}_x\left(\frac{L}{2}, t\right) \tag{1.14}$$

$\hat{d}$ is operator electric dipole for the qubit. If the dipole of the qubit is facing the x direction with the field, we can write $\hat{d} = d_x\left(\hat{\sigma}_x\right)$ with d_x being the magnitude of dipole of the qubit. In general, $\hat{d}$ can be expressed as;

$$\hat{d} = d_x\left(\hat{\sigma}_+ + \hat{\sigma}_-\right) \tag{1.15}$$

$\hat{\sigma}_+$ & $\hat{\sigma}_-$ being the creation and annihilation operator of the qubit. For second quantization, the electric field is in direct proportion to $\hat{E} \propto \left(\hat{a}^\dagger + \hat{a}\right)$. The interaction Hamiltonian can now be reconstructed with g being the qubit-resonator coupling strength as;

$$\hat{H}_{interaction} = g\left(\hat{\sigma}_+ + \hat{\sigma}_-\right)\left(\hat{a}^\dagger + \hat{a}\right) \tag{1.16}$$

[1] Imagining the field in a classical way

Putting ourselves in the limit where it is permissible to do rotating wave approximation (RWA) i.e. neglecting interactions that do not conserve the number of excitation;

$$\hat{H}_{interaction} = g\left(\hat{\sigma}_{+}\hat{a} + \hat{\sigma}_{-}\hat{a}^{\dagger}\right) \tag{1.17}$$

We now have the Hamiltonian that can describe the qubit-cavity combined system.

$$\begin{aligned}\hat{H}_{total} &= \hat{H}_{qubit} + \hat{H}_{cavity} + \hat{H}_{interaction} \\ &= \frac{1}{2}\omega_q\hat{\sigma}_z + \omega_c\left(\hat{a}^{\dagger}\hat{a} + \frac{1}{2}\right) + g\left(\hat{\sigma}_{+}\hat{a} + \hat{\sigma}_{-}\hat{a}^{\dagger}\right)\end{aligned} \tag{1.18}$$

This is called Jaynes-Cummings Hamiltonian $\hat{H}_{JC}$ [6, 7, 8], where ω_q and ω_c are qubit and cavity frequency respectively.

In a situation where the qubit-cavity coupling strength is far greater than the detuning i.e. $\Delta = |\omega_q - \omega_c| \ll g$, the energy of the system is hybridized and a vaccum Rabi frequency of $\sqrt{n}g\ /\ \pi$ is opened up with $n = 1, 2, 3\ldots$ being the resonator modes. Excitations are coherently exchanged between the cavity and qubit in this regime. Although this can be considered desirable for some multi-qubit gate operations, such interactions alter the qubit state when energy is bartered between the cavity and the qubit directly, consequently making it unfavourable in the context of not altering the quantum state while trying to probe it or during the readout.

Dispersive Regime

If the qubit-cavity is far more detuned compared to their coupling strength, i.e. $\Delta \gg g$, no longer do the two systems engage in direct energy exchanges. The Hamiltonian in this region of $g\ /\ \Delta \ll 1$ can be approximately solved using second order perturbation[9] in the limit of few photon in the resonator or the "dispersive approximaton". In doing that, the Hamiltonian looks like;

$$\begin{aligned}\hat{H}_{disp} &= (\omega_c + \chi\sigma_z)\left(a^{\dagger}a + \frac{1}{2}\right) + \frac{1}{2}\left(\omega_q + \chi\right)\sigma_z \\ &= (\omega_c + \chi\sigma_z)\left(a^{\dagger}a + \frac{1}{2}\right) + \frac{1}{2}\tilde{\omega}_q\sigma_z\end{aligned} \tag{1.19}$$

where $\chi = g^2\ /\ \Delta$ and $\tilde{\omega}_q = (\omega_q + \chi)$.

We can see from E.q(1.19) that depending on the state, both the frequencies of ω_q and ω_c gets pushed. χ is the frequency shift depending on the qubit state and this is called "dispersive shift". This asymptotically longitudinal interaction resulting in a shift in ω_c yields a quantum non-demolition(QND) measurement where the cavity resonance frequency changes from it's natural tone to different frequencies depending on the state of the qubit and by detecting this shift , we get the idea of which state the qubit belongs to at tht point in time.

A "Lamb shift" is experienced in the qubit frequency as well. From 1.19 we can see a shift of χ in ω_q where $\tilde{\omega}_q = \omega_q + g^2\ /\ \Delta$ caused by the resonator's vacuum fluctuations.

1.3.1 Dispersive QND readout of qubits

When resonator photon number is limited to a small number i.e when the qubit state is not washed out, depending on the qubit's state, ω_c is jostled either towards $+ve$ or in the $-ve$ direction. If the qubit is in its ground energy level, the resonance frequency of the cavity ω_c will shift away from ω_q ($\omega_c - \chi$ as Figure1.8). At this point, if the qubit switches state to $|1\rangle$ from $|0\rangle$, the

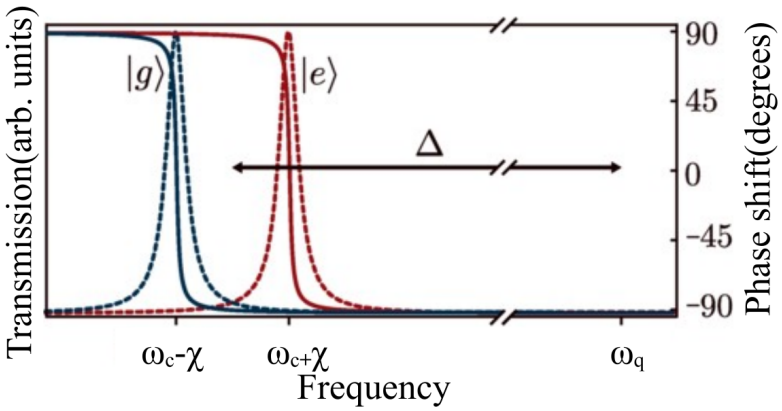

Figure 1.8: Cavity transmission(dashed lines) and corresponding phase shifts(solid lines) for the states of the qubit(ground and excited states are represented by blue and red respectively).[10]

cavity resonance frequency will shift by an amount of 2χ towards ω_q (to $\omega_c + \chi$ in Figure1.8). $2\chi = 2g^2 \,/\, \Delta$ is the shift between the two computational states. Observing this change in resonance frequency provides us the readout information about the qubit state.

It can be demonstrated that we can indeed perform a readout with a very powerful cavity tone. However, this approach will most certainly not result in a QND measurement.

If the photon number $n = a^\dagger a$ in the cavity transcends "critical photon number", dispersive Hamiltonian in E.q.(1.19) is a valid approximation no further. So, an upper limit on the power level of the cavity probe signal that should be maintained is established by the critical photon number[1].

[1]This is an approximation

Chapter 2

Qubit Control and Readout

To control and operate the qubit within its two-state computational subspace, to get the reflected signal back from the cavity, and to be able to successfully determine its state, we need specifically engineered solutions in the peripheral ecosystem of the qubit-cavity duo. Transmon's resonance frequency lies in the microwave region, so does that of the engineered cavity[1]. It requires the programmed pulses for characterisation, computation, and read-out signal to be modulated and demodulated within the microwave frequency range.

As we are trying to control the qubit using light-matter interaction[11] with electromagnetic wave, any allowed excitation due to thermal noise is entirely unwelcomed. While dealing with a superconducting qubit i.e. a dissipation-less superconducting oscillator circuit (Figure1.3), although the primary thermal condition to superconductivity for Aluminium is achieved is below 1.3K; to prevent thermal excitation and to make sure initially level $|0\rangle$ is populated, $k_{\mathrm{B}}T \ll \hbar\omega_{01}$(Figure1.4) has to be maintained. Thus, for our system $T < 50$ mK is maintained, ideally at 10 mK $< T < 20$ mK.

2.1 Imperativeness of Radio frequency engineering

Both in cryogenic and room temperature peripherals of a superconducting quantum processor i.e. qubit, radio-frequency(RF) components including transmission lines , high electron mobility transistors(HEMTs), attenuators, circulators along with others come with specific requirements to fulfill. Some of the most significant segments of a qubit control system is;

- Construction of pulses and carrier waves
- Control and readout pulse modulation and demoduation
- Mixing
- Signal amplification and attenuation
- Signal retrieval
- Analog to digital(AD) and digital to analog(DA) conversion
- Signal processing

and with each of these, the significance of RF engineering in superconducting qubit systems becomes multidimensional.

[1] ω_q&ω_c

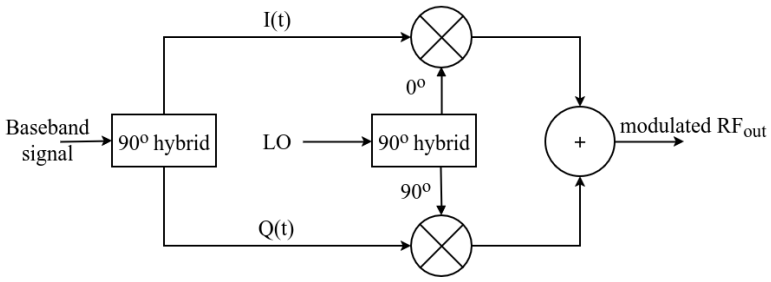

Figure 2.1: I/Q modulation(Homodyne) and mixing circuit schematics.

2.2 Modulation and Demodulation Scheme

In the superconducting qubit control instruments, in order to modulate a pulse coming out of an arbitrary waveform generator(AWG) over the carrier frequency from a local oscillator(LO) (Figure2.1), in-phase quadrature(I/Q) modulation is used. The terms "in-phase" and "quadrature" describe two sinusoids that are 90° out of phase and have the same frequency, having one of them as a reference or "in-phase". By convention I is considered to be the $cosine$ signal and Q as the $sine$ one. The principal defining feature of I/Q signals is that they are amplitude-modulated as oppose to being modulated by frequency or phase. Nonetheless, I/Q modulation varies considerably if compared to the usual amplitude modulation(AM) approach. I and Q signals by themselves are not really noteworthy, though a fascinating event takes place when the I and Q waves get combined. It becomes evident that any modulation type is possible to be accomplished by just altering amplitudes of the I and Q waves and then summing them up.

With the local oscillator(LO) generating a carrier sinusoid of $V_{LO} = \cos(\omega_{LO} t)$ the modulated outputV_{RF} will be;

$$V_{RF} = I(t)\cos(\omega_{LO} t) + Q(t)\sin(\omega_{LO} t) \tag{2.1}$$

The outstanding advantage of using an I/Q mixing technique can clearly be recognized from E.q.(2.1) that not only the amplitude but the phase as well can be altered in real time by controlling two quadrature individually.

2.2.1 Homodyne Modulation

In an analog homodyne modulation or demodulation, the LO is taken as the carrier frequency. If the carrier frequency is ω, the LO frequency will be set directly at $\omega_{LO} = \omega$.

A typical schematic for homodyne modulation is given in the above figure(Figure2.1).The LO signal is phase shifted by π / 2 and introduced into two separate mixers[12]. Where from E.q(2.1), if the amplitude is A and the phase is Θ;

$$A \propto \sqrt{I^2 + Q^2} \tag{2.2}$$

$$\Theta = \arctan\left(\frac{Q}{I}\right) \tag{2.3}$$

If we try to drive many channels with various frequencies, we will need separate LO sources, which may limit hardware flexibility and make the system more resource-intensive.

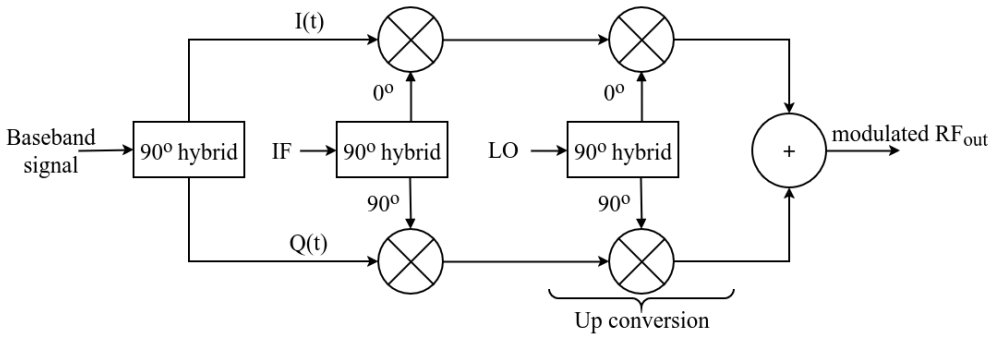

Figure 2.2: Heterodyne modulation with an intermediate frequency(IF) followed by an LO.

2.2.2 Heterodyne Modulation

In heterodyne modulation, the pulse is initially modulated over an intermediate frequency (IF) and then up converted by the LO(Figure2.2). If K is a constant accounting for conversion losses and A_{out} is the amplitude of the RF;

$$\begin{aligned} V_{RF} &= KV_{IF}V_{LO} \\ &= 2A_{out}\cos(\omega_{IF}t)\cos(\omega_{LO}t) \\ &= A_{out}\cos\{(\omega_{LO}+\omega_{IF})t\} + A_{out}\cos\{(\omega_{LO}-\omega_{IF})t\} \end{aligned} \tag{2.4}$$

Three port mixer and up conversion

A three-port mixer(Figure2.3) uses a non-linear element to add or subtract the frequencies of two input signals. Every heterodyne RF transmitter, receiver, or transceiver system contains an RF microwave mixer, which is required to convert base-band signals into RF in a transmitter or RF into base-band signals in a receiver. Three ports of a mixer are;

- IF or baseband port
- LO port
- RF port

In a transmitter, signals are sent into a mixer's LO and IF ports in order to produce an output at the RF port in a process known as up-conversion. In contrast, when utilized in a receiver,

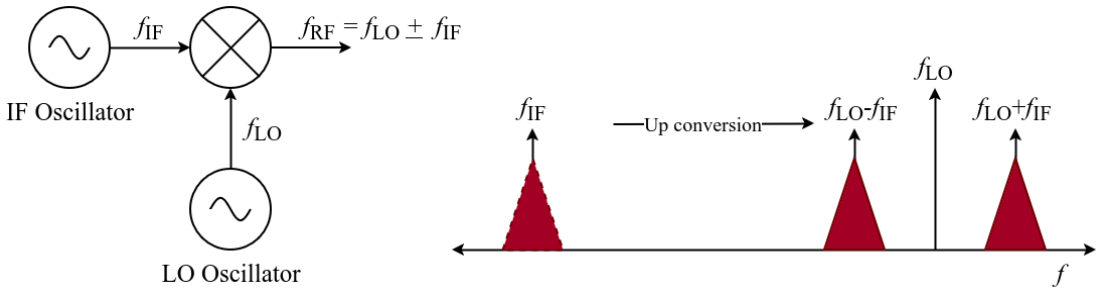

Figure 2.3: Three port mixer and up-conversion in a transmitter.

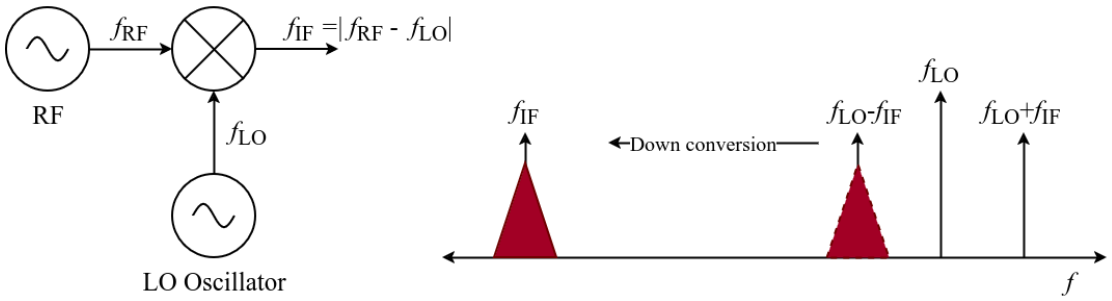

Figure 2.4: Three port mixer and down-conversion in a receiver.

signals are fed into a mixer's LO and RF ports, which produce an output at the IF port through a process known as down-conversion(Figure2.4). The usual scheme of pulse modulation and RF generation in the qubit control system is described chronologically in the figure(Figure2.5).

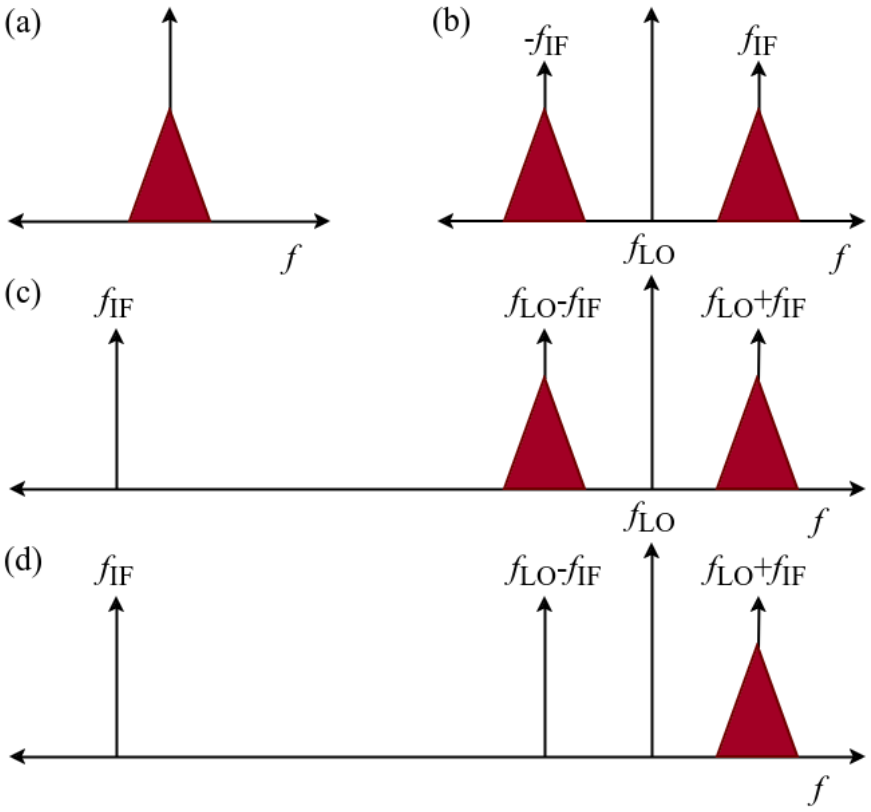

Figure 2.5: **Modulation Scheme:** (a) base-band pulse(in red); (b) base-band pulse modulated over the intermediate frequency; (c) IF up-converted to LO±IF; (d) Single side-band(SSB) modulation with upper side-band(USB) permitted.

The pulse is initially modulated on an intermediate frequency (IF) independently for the I and Q channels, and then both I and Q are routed to an up-converter to be up-converted by LO. The channels are then aggregated to produce a particular modulation in the final RF output.

When it comes to demodulating an intercepted or received RF to obtain the base-band pulse, the process is identical but in reverse.

Advantages of heterodyne modulation

One of the disadvantages of a homodyne system was that it needed individual LO sources for each channel required. When we are speaking of microwave modulation in the GHz domain, having all those tunable LO oscillators makes the system less flexible and inefficient in terms of energy, economic feasibility, and other resources. Heterodyne modulation allows us to initially modulate with an intermediate frequency of ω_{IF} and then LO channel up-converts it with ω_{LO}. So the same LO channel can be used for multiple IF frequencies at the same time, and we will only require individual IF transmitters and receivers in the MHz range to get multi-mode transmission. We also have the requirement of sweeping the carrier frequency, and in most cases, it spans within the MHz range. In such cases, trying to sweep the LO within MHz becomes far less accurate and hectic for the system. With an IF, we can have the LO fixed and sweep the ω_{IF} with far greater resolution in the system.

2.3 Readout Retrieval and Digital Signal Processing

As discussed in Sec.1.3.1, QND readout is achieved by probing the cavity and analyzing the readout(RO) signal in order to get information about the position and phase of the qubit. Focusing our attention on probing the cavity to get the readout, we can perform this either with transmitted wave from the cavity or with reflected wave. In our setup, we are performing a reflected wave readout, and the signal processing path is shown in the figure below.(Figure2.6). In the readout circuit measuring the reflection, the best state discrimination can be accomplished by setting up the system so that the separation is maximum in the I-Q plane, i.e., the in-phase and

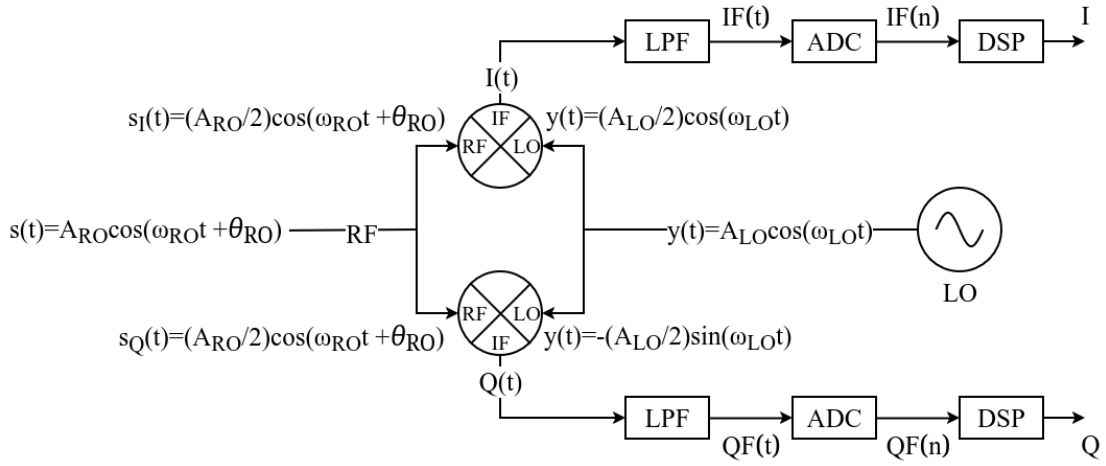

Figure 2.6: Readout path schematic with low pass filter(LPF), analog to digital converter(ADC) and digital signal processor(DSP).

quadrature voltage components. With the cavity probe frequency ω_c defined, the quantum dynamics of the qubit can be mapped using classical electrodynamics and the phase of the readout signal as shown(Figure1.8).

Readout event is done by directing a brief microwave tone towards the cavity at cavity frequency ω_c and intercepting the reflected signal;

$$s(t) = A_{RO} \cos(\omega_{RO} t + \theta_{RO}) \tag{2.5}$$

where the carrier frequency for probing the cavity is ω_{RO}. Qubit state dependent amplitude is A_{RO} and phase is θ_{RO}. If we try to write down a complex representation;

$$s(t) = Re\{A_{RO} e^{j(\omega_{RO} t + \theta_{RO})}\} \tag{2.6}$$

with Re taking the real part from the expression. Evolving from E.q(2.6), we get;

$$s(t) = Re\{A_{RO} e^{j\theta_{RO}} e^{j\omega_{RO} t}\} \tag{2.7}$$

where the phasor is $A_{RO} e^{j\theta_{RO}}$. The in-phase and quadrature component I and Q are denoted by the phasor as;

$$\begin{aligned} A_{RO} e^{j\theta_{RO}} &= A_{RO} \cos\theta_{RO} + j A_{RO} \sin\theta_{RO} \\ &= I + jQ \end{aligned} \tag{2.8}$$

Using E.q(2.8) we can determine A_{RO} and θ_{RO}.

2.3.1 Digital Signal Processing(DSP)

The intercepted signal with frequency ω_{RO} is down converted with LO tone of frequency ω_{LO} giving two quadrature at the intermediate frequency ω_{IF} at $\pi/2$ phase with each other. The signals are then sampled for both I and Q channels in two different analogue to digital converter(ADC). Sampling frequency is kept at least two times or greater than the signal frequency

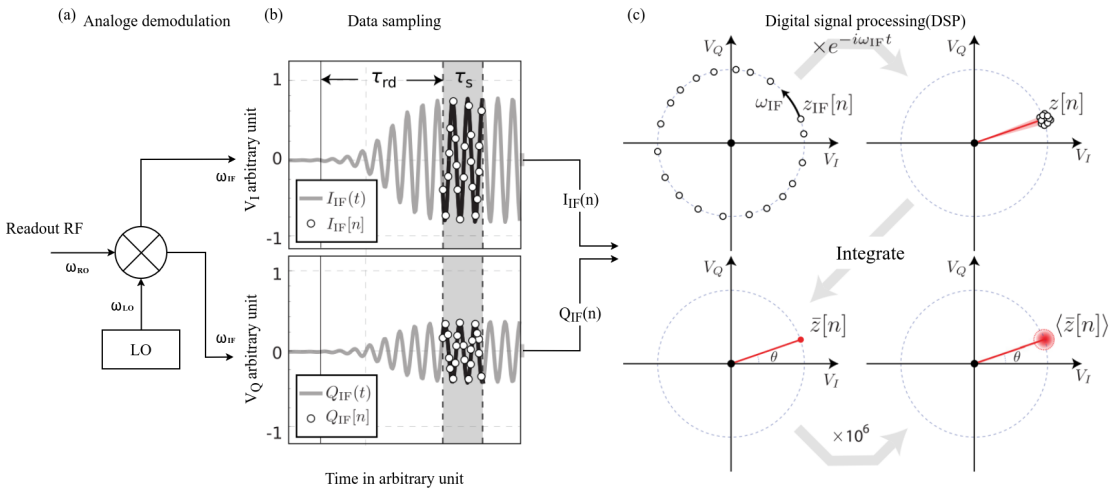

Figure 2.7: Sampling and processing of the readout signal[2].

in order to get rid of aliasing effect[13]. The signal is given some time τ_{rd} to let the transient response pass and sampled through a sampling time τ_s(Figure2.7). The white dotted sampled traces(Figure2.7b) are processed and avarage data points are ploted in IQ plane. To gather the statistics of readout efficiency, or, the single-shot readout fidelity, a substantial amount of (I, Q) datapoints are gathered, providing a 2D-histogram with a Gaussian distribution spread (Figure2.7c) caused by noise.

2.4 Qubit Dynamics and State Manipulation

2.4.1 Bloch Sphere Representation of a Two Level System

Representation of a two level quantum system such as a qubit, requires exploring the idea of a unit sphere named "Bloch sphere". A Bloch vector portraying a quantum superposition state of $|\Psi\rangle = \alpha|0\rangle + \beta|1\rangle$ on Bloch sphere is shown in figure(Figure2.8). Assuming that a Bloch sphere is depicting the Earth, the arctic pole denotes $|0\rangle$ and the antarctic pole represents level $|1\rangle$. In normalised superposition states like $|\Psi\rangle$, the Bloch vector has unit modulus i.e. $|\alpha|^2 + |\beta|^2 = 1$ that originates from the nucleus of the sphere and goes to the circumference. Polar north and south are joined via z-axis. As it serves as the quantization axis of the qubit for states $|0\rangle$ and $|1\rangle$ in the qubit eigenbasis, it is known as the "longitudinal axis". The "transverse plane" and "transverse axes" are the x–y plane with the x and y axes. According to our convention, state $|0\rangle$ at polar arctic represents polarisation $p = +1$ level, $|1\rangle$ at the polar south aligns to $p = -1$ and any state on x-y equatorial plane corresponds to $p = 0$. Similarly, the angles θ and φ can be used

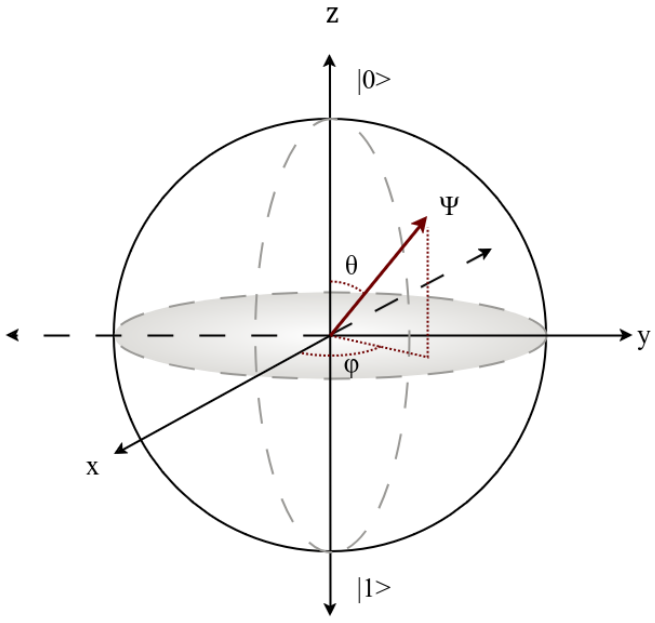

Figure 2.8: Bloch sphere depiction for a two state system with the wave-function as a Bloch vector(in red) $|\Psi\rangle = \alpha|0\rangle + \beta|1\rangle$ in a superposition state.

to describe quantum states as well. With everything defined, we can write the wave-function as;

$$\begin{aligned} |\Psi\rangle &= \alpha\,|0\rangle + \beta\,|1\rangle \\ &= \cos\frac{\theta}{2}\,|0\rangle + e^{j\varphi}\sin\frac{\theta}{2}\,|1\rangle \end{aligned} \tag{2.9}$$

Bloch vector remains stable on the Bloch sphere in a "rotating frame picture". In superconducting qubits, state $|1\rangle$ possesses greater amount of energy than state $|0\rangle$, causing the Bloch vector to rotate around the z-axis at the qubit frequency in a stationary frame. To simplify the visualisation, we instead make the reference frame rotate around z-axix with frequency of ω_q to make the Bloch sphere appear stationary.

2.4.2 Qubit Longitudinal Dynamics: Excitation and Relaxation

To initiate longitudinal rotation of a qubit on the Bloch sphere, an X_θ or Y_θ pulse can be used that rotates the qubit about x or the y axis respectively at an angle of θ. These interactions are called transverse interaction either about x or y axis of the qubit with it's control environment. Longitudinal rotation can either be pulse driven or spontaneous.

Pulse driven excitation

In order for us to get the qubit from it's initial ground level $|0\rangle$ to the excited $|1\rangle$ level, an X_θ or Y_θ pulse can be used with $\theta = \pi$ i.e. X_π or Y_π pulse, so that a turn of π either around the x or the y axis can be executed with which the qubit will end up at it's excited state. For our regular qubit manipulation, we prefer X_θ pulse to rotate the qubit by an angle θ around the x axis, so to get the excitation X_π pulse can be used. As illustrated in figure(Figure2.9), a π pulse either about X or Y gets the qubit to it's $|1\rangle$ excited state. A consecutive π pulse thus should get the qubit back to state $|0\rangle$.

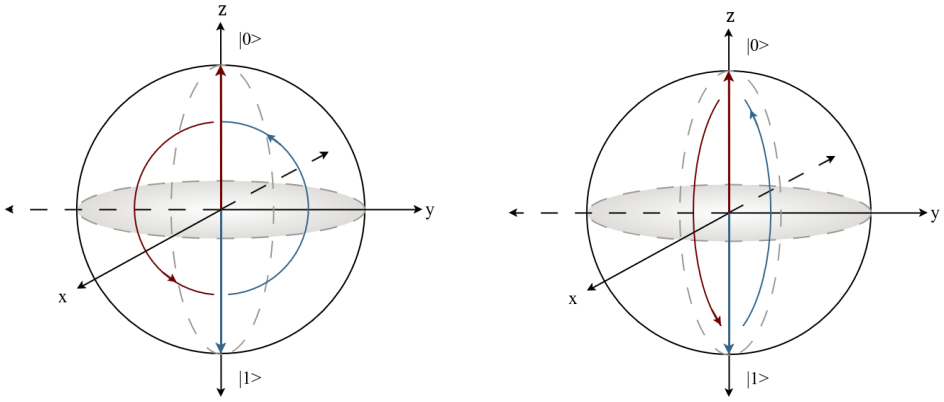

(a) Excitation(red), down transition(blue) due to X_π pulse along x axis and relaxation(blue) due to energy loss, on $y-z$ plane

(b) Excitation(red) down transition(blue) due to Y_π pulse along y axis and relaxation(blue) due to energy loss, on $x-z$ plane

Figure 2.9: Longitudinal transitions and spontaneous relaxation due to transverse interaction.

Spontaneous rotation and qubit relaxation

The discussed transitions in "Pulse driven excitation", can also happen without any intended drive pulse. A transverse interaction can possibly be raised due to thermal noise in the system and subsequent energy exchange depolarizing the qubit. Depolarization generally relates to both an up transition rate $\Gamma_\uparrow$ from $|0\rangle$ to $|1\rangle$ and a down transition rate $\Gamma_\downarrow$ for the reverse transition leading the total transition rate to be;

$$\Gamma_1 = \frac{1}{T_1} = \Gamma_\uparrow + \Gamma_\downarrow \tag{2.10}$$

where T_1 is the $1\ /\ e$ decay time. T_1 signifies the characteristic time for the population reaching to a steady-state value.

As discussed in the beginning of this chapter, with temperature T set in such a way that resists any thermal excitation i.e. the Boltzmann factor $e^{(-\hbar\omega_q/k_\mathrm{B}\mathrm{T})}$ suppress $\Gamma_\uparrow$ exponentially. This makes spontaneous up-transition quite unlikely as the qubit barely gathers enough energy for it but it interacts with the environment loosing it's energy or cooling down with a down-transition i.e. "Relaxation" rate of $\Gamma_\downarrow$ leaving us with an evolved form of E.q.(2.10) [14, 15]

$$\Gamma_1 = \frac{1}{T_1} = \Gamma_\downarrow \tag{2.11}$$

2.4.3 Qubit Transverse Dynamics: Pure Dephasing

Pure dephasing happens with depolarisation on the equatorial plane of the Bloch sphere. This goes by the name "pure dephasing" to differentiate it from various phase disrupting processes including energy excitation and relaxation. Depicted below(Figure2.10), pure dephasing arises from longitudinal noise being coupled with the qubit through it's z axis. These disturbances result in fluctuations of the frequency of the qubit ω_q from the frequency of the rotating frame i.e. ω_d. This pushes the qubit Bloch vector to either precess ahead or retreat with respect to the frame of reference. It makes sense to envision numerous identical preparations of the Bloch vector oriented towards the x-axis. Bloch vector's net fanning-out on the equatorial plane is the result of stochastic variations of qubit frequency, which provide a distinct precession frequency for every single instance. This ultimately causes the azimuthal angle φ to completely depolarize at a rate

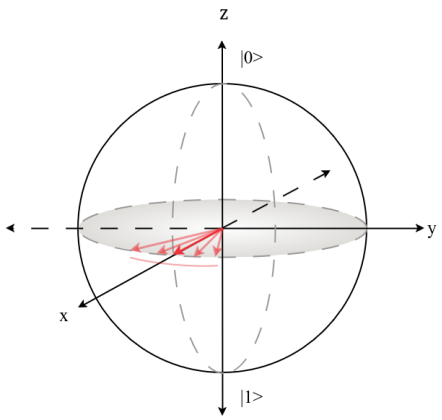

Figure 2.10: Dephasing of a qubit state on x-y plane due to longitudinal noise.

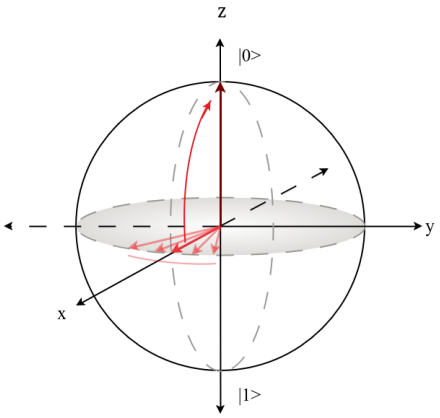

Figure 2.11: Transverse relaxation of a qubit state.

of Γ_φ. The differences between energy relaxation and pure dephasing are significant in a few ways. First of all, pure dephasing does not coincide with resonance like energy relaxation; noise across all frequencies are capable of altering the qubit frequency and induce dephasing. Hence, wideband noise affects qubit dephasing. Secondly, pure dephasing is inherently "reversible" due to its elastic nature (no energy interchange with the environment). That is, by using unitary operations, such as dynamical decoupling pulses, it is possible to mitigate dephasing while preserving quantum information.

2.4.4 Transverse Relaxation of Qubit

Transverse relaxation describes phase breaking of a superposition state or a diminishment of coherence. Suppose a superposition state $|\Psi\rangle = \left(1 / \sqrt{2}\right)(|0\rangle + |1\rangle)$ which is facing the x axis on xy plane of the Bloch sphere(Figure2.11). Decoherence is caused by both longitudinal and transverse noises in parts. Interaction through the longitudinal axis results in pure dephasing of the qubit at a rate of Γ_φ on equator and then transverse noise induces energy relaxation of superposition state and makes the Bloch vector face the polar apex $|0\rangle$ at a rate of Γ_1. Thus we get;

$$\Gamma_2 = \frac{\Gamma_1}{2} + \Gamma_\varphi \tag{2.12}$$

Transverse relaxation T_2 is ascertainable using Ramsey interferometry.

Chapter 3

Experimental Arrangements

In this chapter, we are about to discuss the required experimental setup for characterisation experiments. Let the overall arrangement be boiled down to two segments depending on their operational temperature range .

- Cryogenic setup
- Room temperature setup

3.1 Cryogenic Setup

As discussed in chapter 2, to probe the qubit keeping it within its computational subspace, the temperature should be maintained below 50 mK. For a transition frequency around 4.2 GHz and

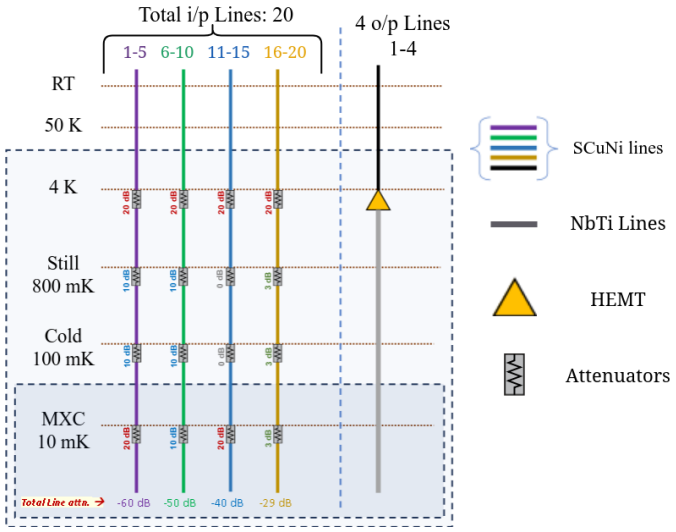

Figure 3.1: **Wiring in the refrigerator:** four sets(illustrated in different colour) of input SCuNi lines, with different line attenuation, five lines in each set; NbTi output line(in grey) with a HEMT.

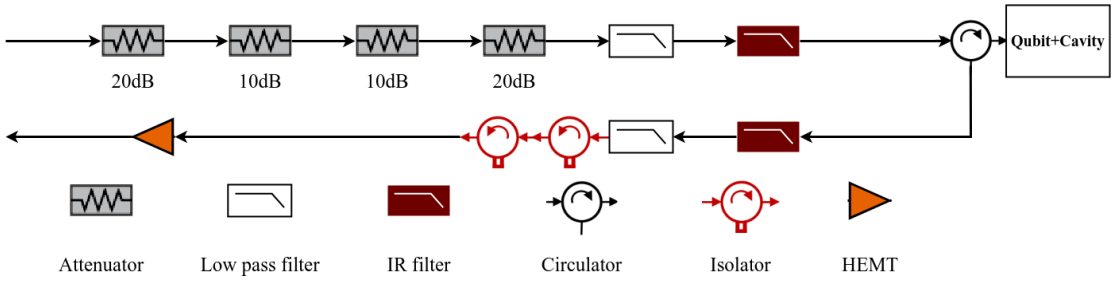

Figure 3.2: Connection schematic to the qubit-cavity system.

we keep it within 10 mK-20 mK. As a result, cryogenics is necessary for our research. A *Bluefors LD250*[1] dilution refrigerator was used for the studies described in this paper. The wiring setup has been illustrated in figure(Figure3.1).

We make sure that the sample is not affected by noise from room temperature component. Qubit and readout line has a 300 K Jhonson-Nyquist noise[16] while entering on top of the fridge. This noise must be heavily attenuated with attenuators. Therefore, attenuators are placed at different stages in the refrigerator such that they only add noise of their temperature further in the chain. The last attenuator is kept at the base plate with a temperature of 10 mK. The connection to the qubit-cavity system using a single input line of 60 dB attenuation is illustrated in figure(Figure3.2). The line has a transmission impedance of 50 Ω. A signal from the input channel eventually goes through a circulator and into the qubit-cavity system. The signal interacts with the system and after that, it reflects. The output line sends the signal from the qubit to the room temperature setup. It goes through isolator to a high electron mobility transistor(HEMT) at the 4 K plate. The HEMT improves the SNR[2]. In certain situations, the possibility to amplify the reflected signal at the base plate temperature has also been investigated. We may utilize nearly quantum-limited amplifiers, called Josephson parametric bifurcation amplifiers[17, 18, 19], to amplify signals at the base plate temperature level.

The notable thing in Figure3.2 is the use of two isolator instead of a Dual-Junction circulator terminated with 50 Ω cryo terminators. Since we did not have 50 Ω cryo terminators, we used another isolator[3] instead.

3.2 Room Temperature Setup

Aside from the cryogenic arrangement, microwave/RF circuits operating at room temperature to create pulses for qubit control and readout are used. We are employing heterodyne setup to create and modulate pulses. In the experimental setup we had a *Rohde & Schwarz ZNL-14*[4] vector network analyzer(VNA); and for programmed pulse generation and readout, we have *Quantum Machine's OPX+*[5] *& Octave* [6] duo.

[1] https://bluefors.com/products/dilution-refrigerator-measurement-systems/ld-dilution-refrigerator-measurement-system/

[2] HEMT amplifies the signal so that room temperature noise does not suppress the signal to a point where it gets lost.

[3] An isolator is a circulator with one port terminated at 50 Ω. As all the other lines are matched to 50Ω, there are no reflections ad an isolator acts like a non-reflective diode.

[4] https://www.rohde-schwarz.com/in/products/test-and-measurement/network-analyzers/rs-znl-vector-network-analyzer_63493-432704.html

[5] https://www.quantum-machines.co/products/opx/

[6] https://www.quantum-machines.co/products/octave/

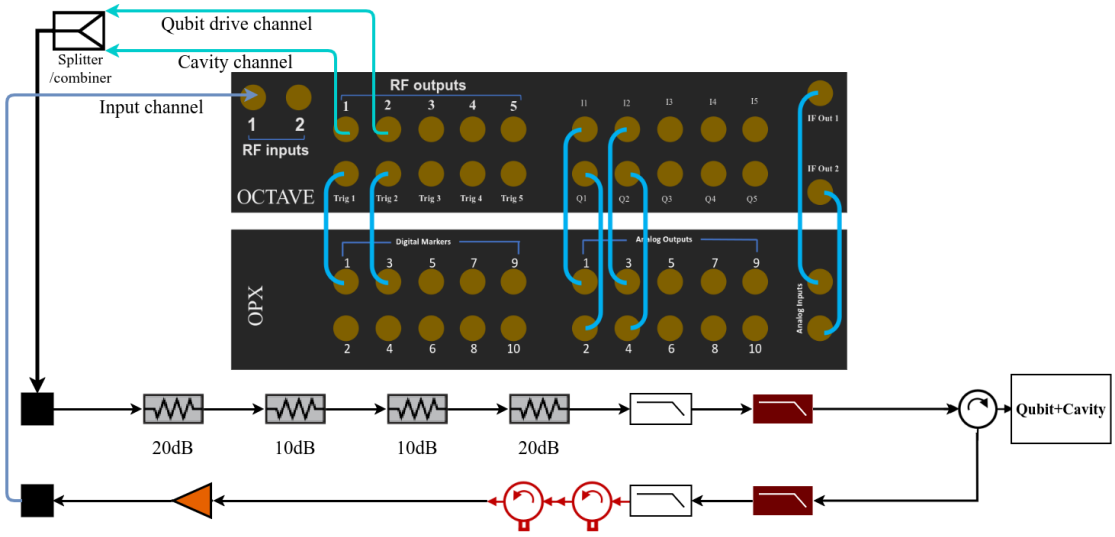

Figure 3.3: Schematic of a Quantum Machine's OPX-Octave duo in room temperature to refrigerator connection.

3.2.1 Standard Qubit Control Room-Temperature Setup

In the conventional arrangement, we adopt the Single Side Band modulation approach, as explained in Sec.2.2.2. Operator-X(OPX) is generating a programmed pulse with appropriate I and Q quadrature with an arbitrary wave-from generator(AWG) and then modulate it over an IF in the MHz range. Then the quadrature are sent over to the up-converter and mixer module Octave as a pair separately for both qubit and cavity at their distinct ω_{IF}. Up-converted by LO and modulated, the signals for qubit and cavity leave the Octave into a combiner [1] as in our qubit-cavity setup, we have the same coaxial line for both the qubit and cavity and the separate qubit and cavity channel gets combined and sent into the fridge.

The reflected wave comes out at the output(Fridge-out) line and gets docked into one of the two input port of the Octave to then get down-converted with the LO it was initially up-converted with. After getting down-converted, the two ports are then sent back to the OPX to then demodulate and retrieve the waveform out of it. OPX processing unit consists of a CPU and an FPGA system which then process the signal. The Octave houses three individual programmable local oscillators, so the choice of number of LO in the set up is hardware limited to three with two input ports for down conversion. With this setup, we can drive three LO oscillators available through RF output 1, 2&3, 4&5.

To ascertain the phase disparity in the reflected signal, the LO tone for the demodulation mixer is obtained from the same RF source as the readout up-conversion mixer. Prior to being sampled and digitized, the demodulated I and Q signals are routed to a low-noise pre-amplifier.

Setup Using VNA

For single tone spectroscopy; and at the same time for component inspection such as impedance checking and RF spectroscopy of elements, we use a vector network analyzer(VNA). A sim-

[1] The three-port RF combiner/splitter distributes power received from the input port equally between the two output ports. The part can also be used to combine signals because of it being a passive device.

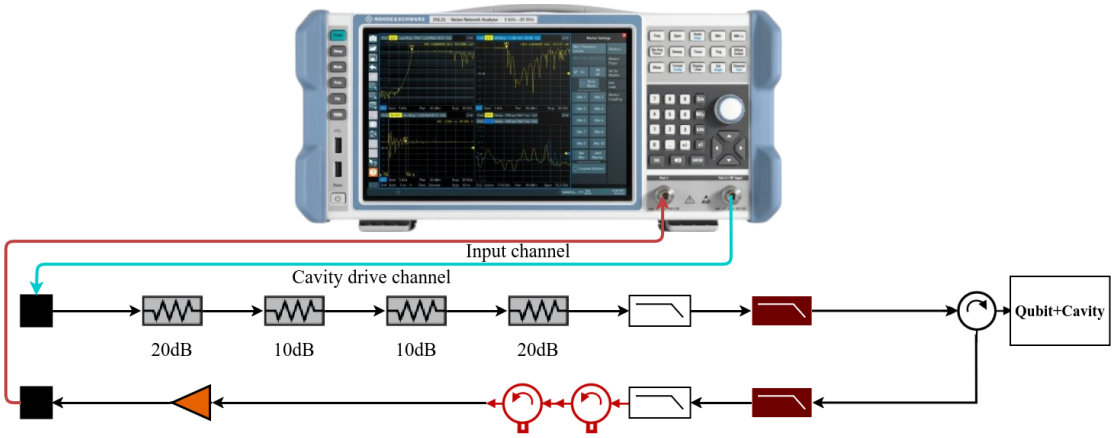

Figure 3.4: Schematic of VNA in room temperature to refrigerator connection for single tone cavity spectroscopy.

ple connection schematic for single tone qubit spectroscopy with VNA is illustrated in the figure(Figure3.4) for our experimental arrangement. The RF output in the VNA is set to a certain desired frequency(LO like) and thereafter an appropriate frequency sweep(IF like) span can be assigned on top of that with output power defined properly. the output from VNA then goes on top of the fridge to the fridge input or drive line. The reflected signal from the fridge output line goes into the input port of the VNA and studied against the generated signal.

3.2.2 S Parameter Analysis Using VNA

In microwave electronics, as it is not possible to have defined open and short circuits in the seance of a traditional network, we can not apply usual Y or Z parameters in microwave circuits. In microwave circuits, we use S or scattering parameters. S parameters are meaningless unless we are aware of the reference impedance's value.

If we now try to examine a simple two-port network with characteristic impedance Z_0 (Figure3.5). The signal at, let's assume, port 1, is capable of being conceptualized as a composite of two waves propagating in opposite directions, incident wave going in(a) and reflected wave coming out(b). Now, a parameter S_{ji} implies the following;

$$S_{ji} = \frac{\text{Normalised reflected wave at j}^{\text{th}}\text{ port } (b_j)}{\text{Normalised incident wave at i}^{\text{th}}\text{ port } (a_i)} \tag{3.1}$$

with b_j = reflected amplitude at j$^{\text{th}}$ port$/\sqrt{Z_{0j}}$; a_i = incident amplitude at i$^{\text{th}}$ port$/\sqrt{Z_{0i}}$.

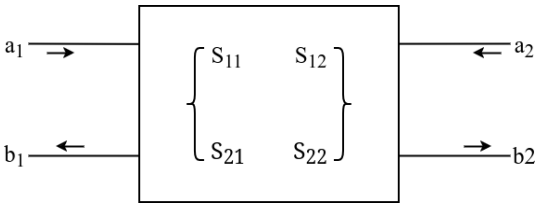

Figure 3.5: Generalised two port network with characteristic impedance Z_0.

The matrix representation of S parameter in this two port network can be written as;

$$\begin{pmatrix} b_1 \\ b_2 \end{pmatrix} = \begin{pmatrix} S_{11} & S_{12} \\ S_{21} & S_{22} \end{pmatrix} \begin{pmatrix} a_1 \\ a_2 \end{pmatrix} \tag{3.2}$$

In our experiment using VNA, we will effectuate S_{21} analysis, where;

$$S_{21} = \frac{\text{Normalised reflected wave at the } 2^{\text{nd}} \text{ port } (b_2)}{\text{Normalised incident wave at } 1^{\text{st}} \text{ port } (a_1)} \tag{3.3}$$

Chapter 4

Experimental Methods

The characterization experiments of a qubit can be streamlined into steps in proper sequence. We, in this chapter will encounter each segments separately one after another until we get our single superconducting qubit system ready to perform computational gate operations.

All of the following experiments are done in the evacuated and cooled down refrigerator as discussed about in Sec.(3.1) below 20 mK.

4.1 Cavity "Punch Out" Spectroscopy using VNA

The key motive of this experiment is to inspect if the qubit is functional or not. We perform a simple single tone cavity spectroscopy using the VNA. We could have used the Quantum Machine's control unit in order to perform this but for the sake of simplicity and for no requirement of programmed pulses, we have used VNA instead. The arrangement using VNA is mentioned in Sec.3.2.1.

The experiment probes the implication of the qubit upon the cavity frequency ω_c. In presence

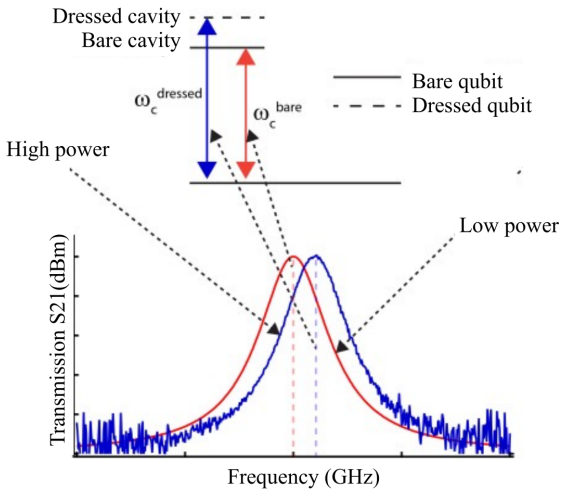

Figure 4.1: Single tone punch out spectroscopy[11].

of the qubit in any of it's energy state, the cavity frequency shifts from it's bare tone ω_c^{bare} to $\omega_c^{dressed}$ which we have addressed so far in a qubit-cavity coupled system as cavity frequency i.e. ω_c.

If we now increase the drive power for the qubit to a stage where the critical current for the Josephson junction is exceeded and the qubit is left functional no more i.e. the qubit is *"punched out"*, we shall notice shift in ω_c and the bare cavity frequency ω_c^{bare} will become the resonance frequency for the qubit which previously was at $\omega_c^{dressed}$. This difference of cavity resonance frequency in single tone spectroscopy between high power and low power drive provides us information about the functionality of the qubit i.e. if it is alive or not.

4.2 OPX and Octave System Calibration

The OPX and Octave system along with the transmission line needs calibration to offset any system potential and to account for the time taken of signal travelling back to the system from the fridge to tune in the signal processing properly. These calibrations lead to finer adjustment in the system for proper operational capability.

4.2.1 Raw ADC Trace

The raw ADC trace experiment works on playing a short readout rectangular pulse to the cavity and with the reflected back wave, constructing a raw tracing without any pre-processing. Any offset DC potential level is thus identified over many iteration and machine configuration is adjusted.

4.2.2 Time of Flight Measurement

We have illustrated(Figure3.3) the signal path from the control system to the cavity-qubit module and back to the control unit. The pulse of-course takes a finite amount of time to travel this finite length of path. And the instrument needs to be properly calibrated for that time of flight to avoid unintended data and misplaced phase in the retrieved and sampled signal. It's the raw ADC trace that along with dc voltage offsets on both I and Q channels, provides us with the time of flight data along it's time axis.

4.3 Frequency Domain Measurement

Though we have started this chapter with a frequency domain experiment in Sec.4.1 and have already got an idea of the cavity frequency in coupled state $\omega_c^{dressed}$ and bare cavity frequency ω_c^{bare}, the experiment was to wash out the qubit states to have an idea of if it was there to begin with. Once we are satisfied with that, we shall limit ourselves only in the coupled system with cavity frequency $\omega_c^{dressed}$, which we will call ω_c from now on.

Now in a qubit-cavity coupled system, we need to find the resonance tone for both the qubit and the cavity. In order to do the experiments, the instrument communication pathway is set up like it was mentioned in figure(Figure3.3).

4.3.1 Single Tone Spectroscopy

In single tone spectroscopy, we probe the cavity with microwave sweeping the frequency in the region the resonance frequency ω_c is in, keeping the qubit undriven in state $|0\rangle$. We already

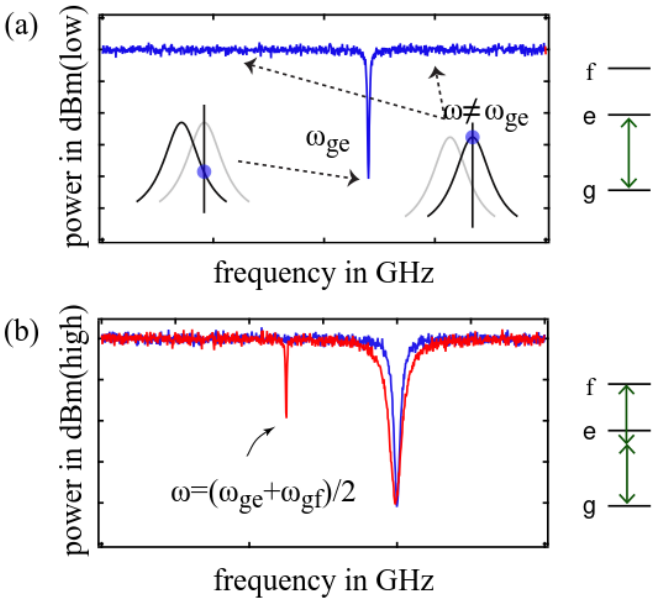

Figure 4.2: (**a**) The cavity transmission during sweeping frequency exhibits a dip corresponding to $\omega_q = \omega_{ge}$ when the cavity is pushed out of resonance. (**b**) For increased power levels(traced in red), the "two-photon transition" is observable as well. Power broadening of the qubit transition is noteworthy[11].

should have a rough idea of what this span could be from the punch out spectroscopy and design parameters of the cavity. Analysing the reflected signal, we should have a variation of amplitude and phase from the I and Q signal to identify the resonance just as discussed in Sec.4.1. the experiments, at their methodically are almost the same but performed on a different instrument without punching out the qubit keeping in mind the power limitation known from that experiment.

4.3.2 Two Tone Spectroscopy

Once we have the cavity resonance frequency ω_c known to us through the single tone measurement, we have to find out the qubit frequency ω_q to construct the qubit drive tone.

To find out ω_q, we drive the resonance tone of the cavity and simultaneously another tone with sweeping frequency in order for the qubit to respond to it and to have the initially grounded qubit at $|0\rangle$ to change it's state to $|1\rangle$. As soon as the qubit does that, it will kick the cavity out of it's earlier resonance frequency ω_c for ground state of the qubit $|0\rangle$ to a new ω_c for qubit excited state $|1\rangle$ as discussed in Sec.1.3.1 in dispersive QND readout. Probing the cavity and analysing the readout pulse, we find out at which frequency the cavity is coming out of resonance(Figure4.2a) i.e at which frequency of the second tone, the qubit is changing its state. This is how we find the qubit transition frequency ω_q[11, 20].

If we administer higher power signal into the system, increasing the available photon number in the cavity, an interesting phenomena of a two photon transition(Figure4.2b) to the second excited level $|2\rangle$ from $|0\rangle$ also becomes visible in the spectrum. While dealing with reflected signal cavity spectroscopy, it is important to analyse both the magnitude and phase in the readout.

4.4 Time Domain Measurement

Now that we know the qubit and cavity frequencies, we can investigate qubit dynamics. Herein, we shall investigate the chronometric assessment of the qubit. Initialization, arrangement and control of the qubit's state, as well as readout, are all required for time domain measurements. The setup employed is discussed in Sec.3.2.1. Following is a quick discussion of some steps.

Initialization- In the present circumstances, initialization is rather straightforward. The system has a lifetime of tens of microseconds, therefore leaving the qubit for about 100 microseconds guarantees with utmost fidelity that it is occupying the ground state.

Preparation and manipulation of qubit states- In contrast to spectroscopy, where signals are constantly sent to assess scattering properties, time domain measurements require precise timing and length of pulses. This suggests that we ought to possess the capability to turn the signals on and off with exacting accuracy. Both the modulation scheme in Sec.2.2 and the qubit dynamics in Sec.2.4 has been discussed and now we will see how they relate to each other through a simple schematic in figure(Figure4.3).

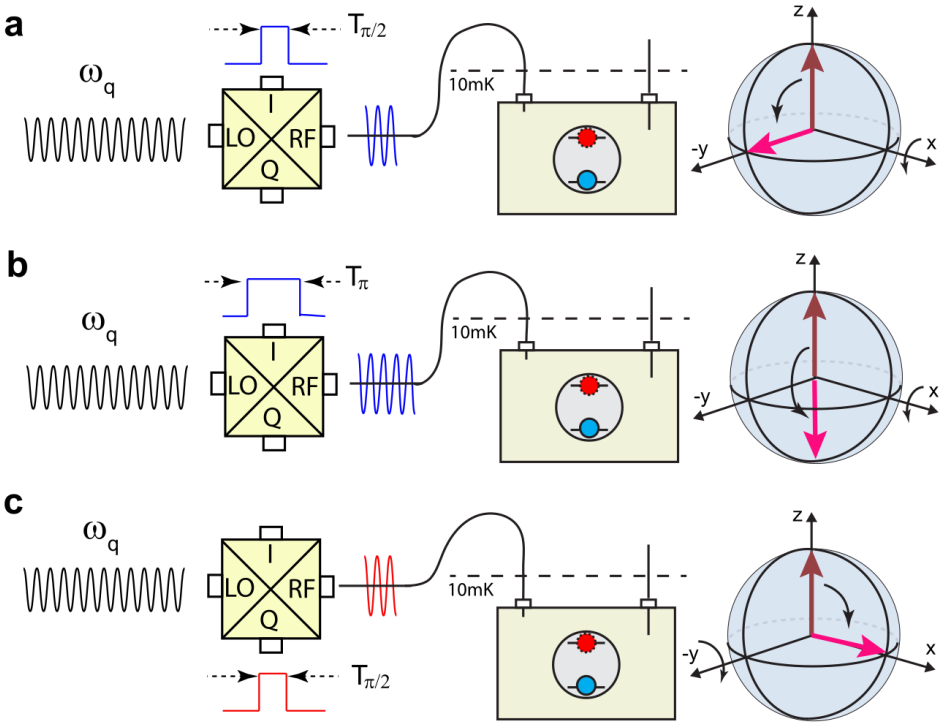

Figure 4.3: **Qubit rotation pulses:** Pulses in the I and Q ports cause rotation in the x and y directions of the Bloch sphere. (a) A $\pi/2$ pulse at port I rotates the qubit in the x direction by $\pi/2$, preparing a superposition state along the y axis. (b) The π pulse along x, i.e an X_π pulse prepares the qubit in an excited state. (c) A $\pi/2$ pulse on Q rotates the qubit about the y axis while preparing it in a superposition along x[11].

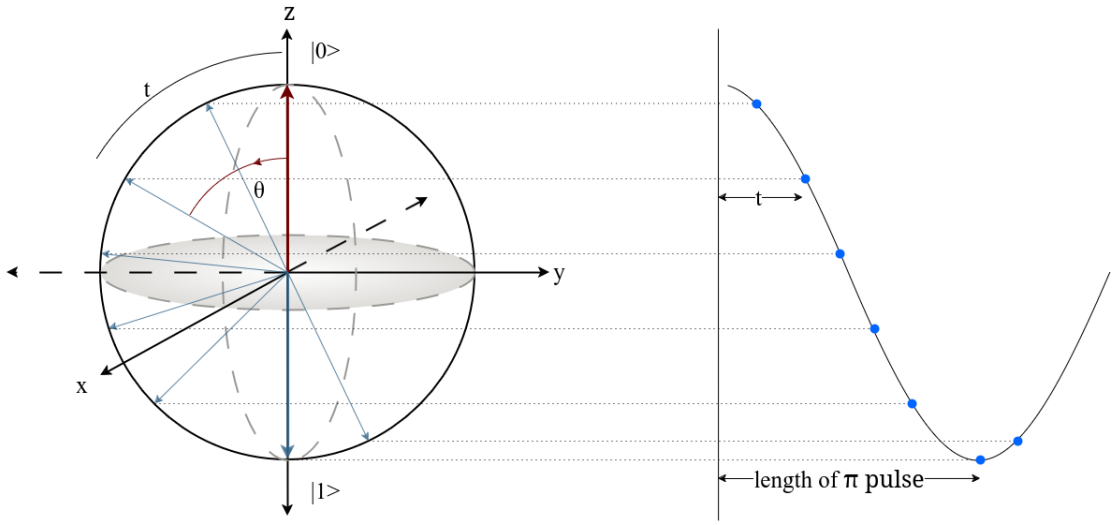

Figure 4.4: Time Rabi measurement and X_π pulse length calibration.

4.4.1 Rabi Oscillation: Time and Power Calibration of Drive Pulses

The inaugural experiment in the temporal domain measurements is to observe Rabi oscillations [21]. The goal here is to be able to accurately construct a transverse θ pulse i.e. an X_θ or a Y_θ computational pulse for state manipulation in terms of power or amplitude and time length.

Time Rabi measurement

In this experiment, X_θ[1] pulse of a certain amplitude kept within reasonable power limit is send to the qubit for different time duration followed by an immediate readout pulse. Readout is analysed in terms of either I(t) or Q(t). In between each pulse played with gradually increasing time length and readout retrieval cycle, the qubit is initialised to $|0\rangle$ using decoherence. The Quantum Machine's OPX has a clock cycle of 4ns so the pulses will have a length of either 4ns or integer multiple of 4ns.

The I(t) or Q(t) value is plotted against the pulse length(Figure4.4) and the length of the pulse needed to perform a π rotation is identified i.e. the length of X_π or Y_π pulse for that specific amplitude as variation in amplitude will result in varying rate of rotation about x or y axis. Let us assume this pulse length turned out to be t_0. As we are dealing with a signal processing unit with clock pulse of 4ns, the time resolution indeed is limited to that. We will further need to calibrate the amplitude as well and run these experiments back and fourth couple of time for finer adjustment.

Power Rabi measurement

In power Rabi, the previously found time length of π pulse t_0 is dialed in the configuration and the control pulse amplitude is made to sweep to yield a varying rotation on the Bloch sphere for varying amplitude or power creates different rate of rotation around x or y axis. In power Rabi measurement, X_θ pulse of time length t_0 but with different and gradually changing amplitude

[1]Or Y_θ for rotations about y axis on the x-z plane.

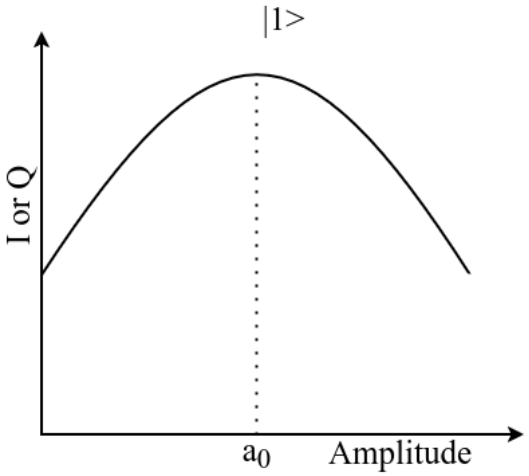

Figure 4.5: Power Rabi plot.

is send to the qubit followed by an immediate readout pulse. Readout is analysed in terms of either I(t) or Q(t). I or Q is plotted against the gradually varying amplitude of the control pulse to obtain the exact pulse amplitude a_0 for the perfect π rotation.

For the finite amount of resolution both in terms of time due to clock pulse and signal amplitude due to resolution in the ADC, proper pulse length and amplitude calibration requires multiple sessions of consecutive time and power Rabi measurement cycle.

4.4.2 Coherence Time; T_1 Measurement

A fundamental attribute that a qubit has is its relaxation time due to its transverse interaction and energy loss to the environment as discussed in Sec.2.4.2. To estimate the lifespan of the qubit, subsequent steps are carried out. Initially, the qubit gets positioned in the excited state with a transverse π pulse. Then we wait for time t before gauging the state with a readout wave delivered to the cavity. We do this for different values of gradually increasing t.

The experiment adopts an arrangement closely resembling that of the Rabi oscillation measurements, though this time with a slightly different pulse sequence compared to the previously employed setup.

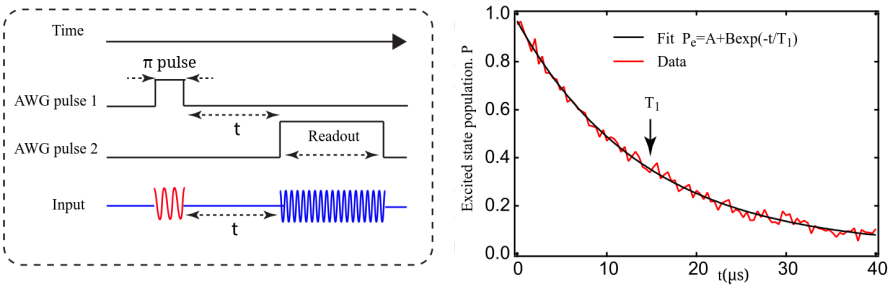

Figure 4.6: T_1 measurement and AWG pulse sequence[11]. AWG pulse1 is a qubit drive pulse on qubit channel, pulse2 is a readout pulse on cavity channel.

The qubit naturally relaxes to the ground state over time(Figure4.6). The data obtained can be fitted to a fading exponential model;

$$I(t) = A + Be^{\left(\frac{-t}{T_1}\right)} \tag{4.1}$$

4.4.3 Ramsey Measurement(T_2^*)

As we now know, our qubit is alive and our pulses are defined, we can thus study the dynamics of dephasing that we discussed in Sec.2.4.3. We use Ramsey measurement to evaluate the dephasing duration T_2^* of the qubit.

The experiment is done by creating an evenly probable superposition state with the utilization of a transverse $\pi/2$ pulse and bringing the Bloch vector along a transverse axis on the equatorial plane from state $|0\rangle$ on the north pole. then wait for time t and send another $\pi/2$ pulse with an immediate following readout to the cavity(Figure4.8).

We do this experiment for gradually increasing time of t and notice where the dephasing angle reaches a value of $\pi/2$ keeping the qubit in the same equal probability superposition state preceding and subsequent to the second $\pi/2$ pulse. The Ramsey curve(Figure4.7) obtained can be defined as;

$$I(t) = A + B\sin(2\pi\Delta_d t + \phi)e^{\left(\frac{t}{T_2^*}\right)} \tag{4.2}$$

The dephasing happens because of the qubit drive frequency being not perfectly set to the accurate qubit frequency or the precision frequency of the Bloch vector or the frame rotation frequency to keep the vector stationary. Due to this, the Bloch vector takes a different frequency which is the drive tone frequency and gets dephased from the frame rotation itself. The detuning of the actual qubit transition frequency ω_{q_o} and the obtained frequency ω_q from the two tone spectroscopy in Sec.4.3.2, i.e the drive tone frequency to the qubit, might be difficult to detect but significant.

Typically, this pulse's carrier frequency is subtly offset intentionally compared to the qubit frequency with a magnitude of $\delta\omega$ consequently leading the Bloch vector to undergo a rotation about the z-axis. Done for the sake of ease, it makes the succeeding Ramsey measurement oscillation easier to examine and analyze.

Examining the dephasing, we can correct the qubit drive tone frequency up to a few kHz compared to the MHz range in two tone spectroscopy in Sec.4.3.2.

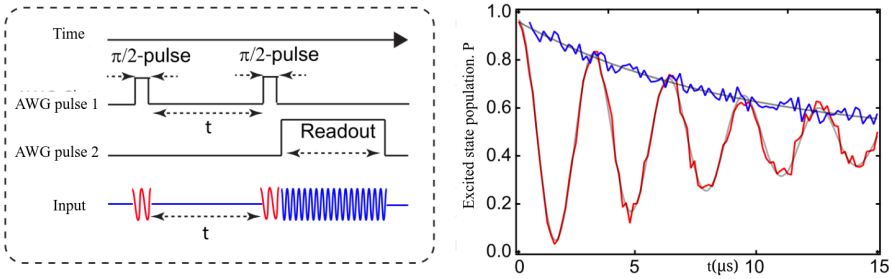

Figure 4.7: The pulse sequence for the Ramsey measurement and plotting pf population/I or Q(red)[11].

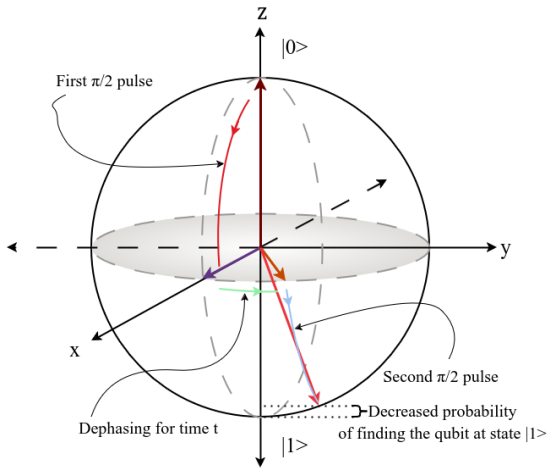

Figure 4.8: Bloch vector dynamics under Ramsey interferometry with $Y_{\pi/2}$ pulses.

4.4.4 Hahn Echo Measurement (T_{2E})

The Hahn Echo (or spin echo) measurement is used to determine the phase decay time T_{2E}. The echo measurement is resistant to detuning and qubit state loss, as the Hahn echo experiment is less sensitive to quasistatic noise. The Hahn echo experiment is done by splitting the waiting time in Ramsey experiment in half, and driving a different π pulse from the second transverse axis.

The pulse sequence can be written as a $X_{\pi/2}$ pulse followed by a $t/2$ dephasing time; a Y_{π} pulse next to it and another $t/2$ dephasing time followed by a $X_{\pi/2}$ derive pulse and immediately measured by a readout(X and Y pulses are interchangeable). The π pulse in the center cancels the slow noise of the qubit. If there is a tiny detunement between the qubit drive and the real qubit frequency, the slow noise is caused by Larmor precession. The measurement can be fitted by a function;

$$I(t) = A + B\sin(2\pi\Delta_d t + \phi)e^{\left(\frac{t}{T_{2E}}\right)} \tag{4.3}$$

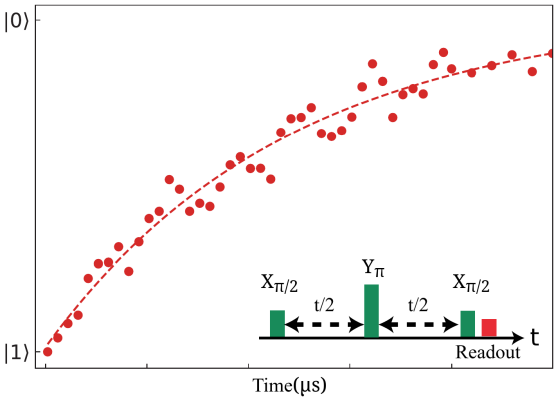

Figure 4.9: Hahn Echo plotting and the control pulse sequence[2].

As echo measurement eliminates slow noise from the qubit-cavity system, it is a more accurate assessment of a qubit's coherence times.

Chapter 5

Experimental Analysis

With the understanding of the experiments discussed in the Chapter4, and the experimental setup described in Chapter3, we now should proceed forward to investigate a single superconducting qubit. The experiments were done on a transmon placed inside a Aluminum cavity developed by TIFR, India.

5.1 Cavity Single Tone Spectroscopy and "Punch Out"

As described in Sec.4.1, the functionality of the qubit was checked. The experiment was done using VNA and again repeated using Quantum Machine's setup. The real part of the S_{21} data is plotted against the frequency(Figure5.1).

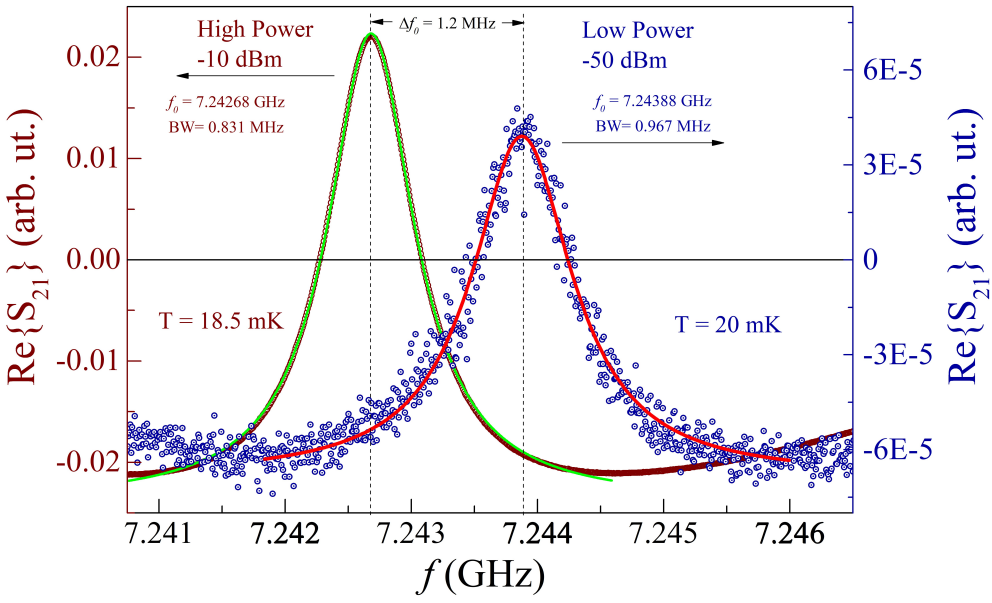

Figure 5.1: **Cavity response** ($Re\{S_{21}\}$) **using VNA:** at low and high powers, blue and browns are data points, curves are fitted with red and green respectively.

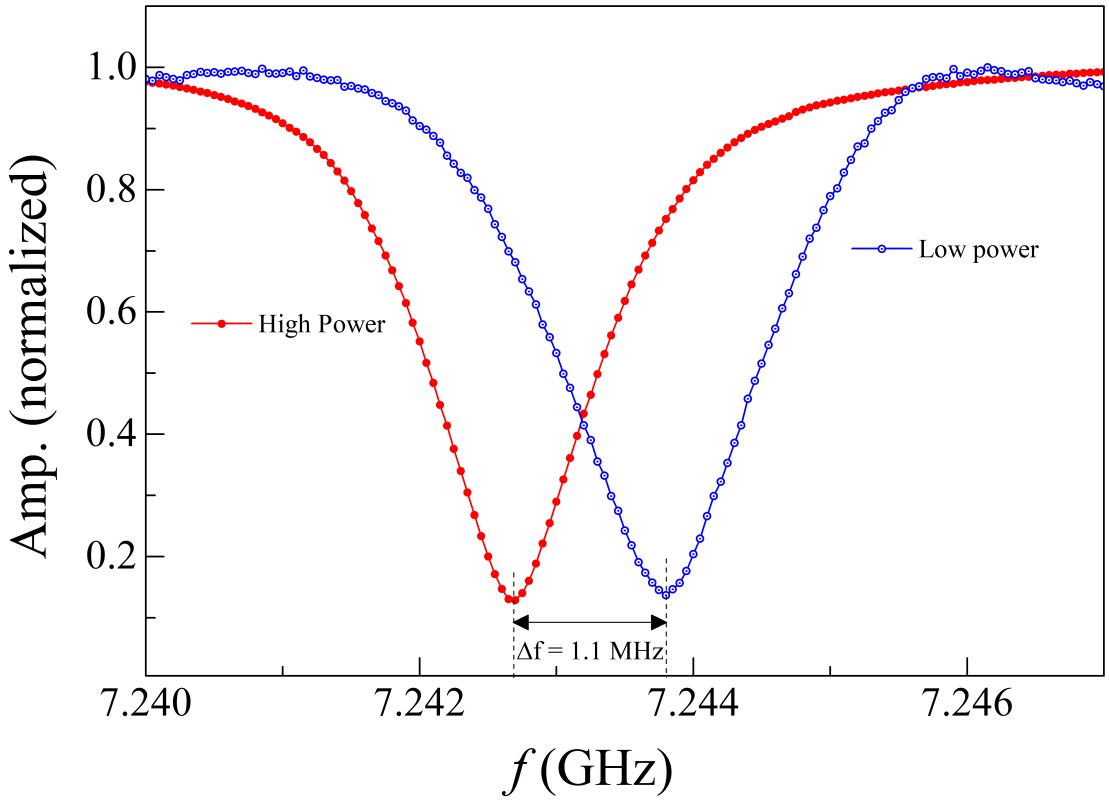

Figure 5.2: Cavity response at low(blue)and high(red) powers using Quantum Machine.

To obtain more information, the real component of S_{21} was fitted to a Lorentzian function;

$$Re\{S_{21}\} = \frac{A}{(x-\omega_c)^2 + \kappa^2/4} \tag{5.1}$$

Herein lies κ standing for the cavity's spectral breadth and ω_c is cavity frequency. This analysis yielded the following data;

- At low (-50 dBm) power, the cavity resonance frequency is 7.24388 GHz with bandwidth 0.967 MHz.
- At high (-10 dBm) power, the cavity resonance frequency is 7.24268 GHz with bandwidth 0.831 MHz.

From figure(Figure5.1), a punchout of the qubit at higher power is observed hence establishing the fact that at low power the qubit is functional and coupled to the cavity. The punchout had a frequency shift of almost 1.2MHz(Figure5.1), the same when observed in Quantum Machine(QM) setup was around 1.1MHz(Figure5.2).

The coupled cavity frequency $\omega_c^{dressed}$ was found to be 7.24388 GHz which in the further studies will be refereed to as ω_c.

A 2D plot(Figure5.3) shows us the punching out of the qubit much more clearly with varying power. The QM setup was used to obtain this plot.

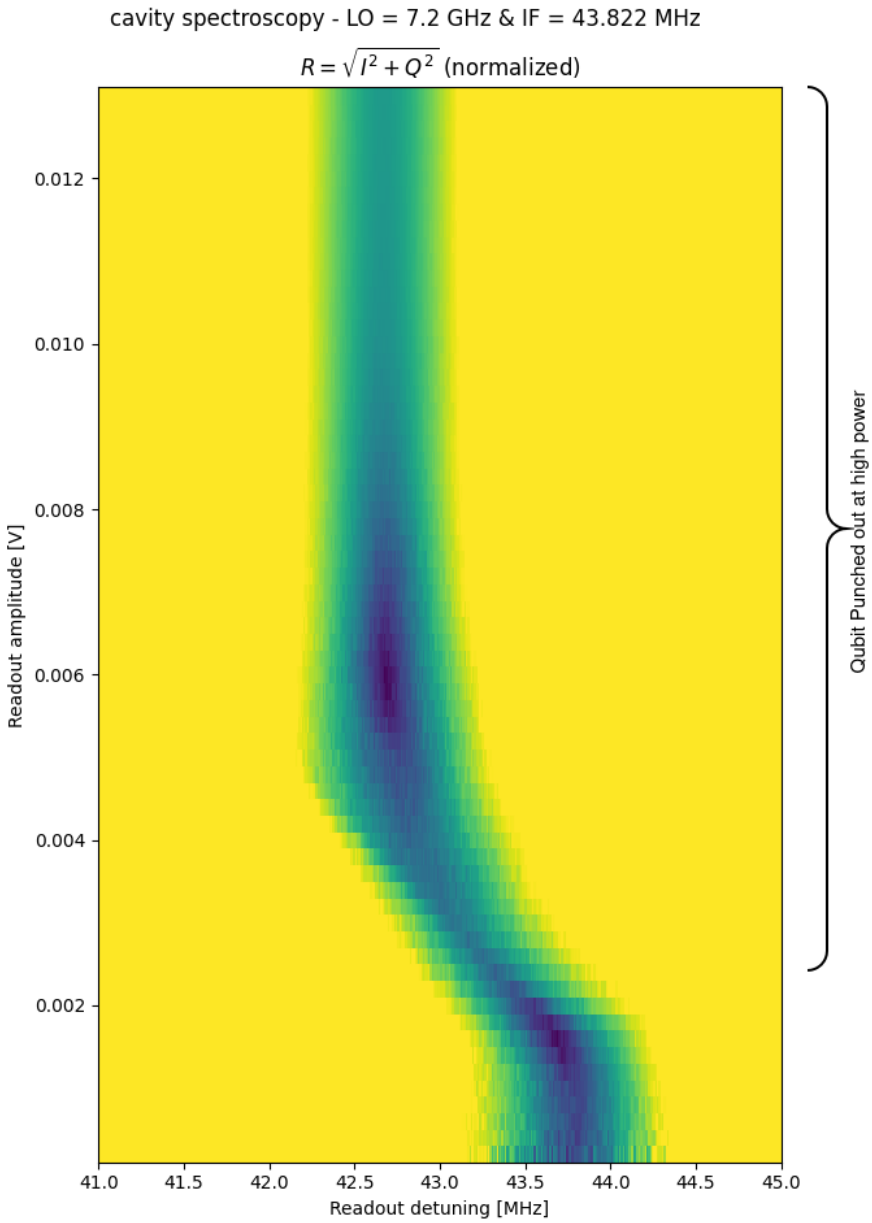

Figure 5.3: 2D plot of single tone cavity spectroscopy. Here readout detuning is the IF value difference of the RF from LO=7.2 GHz where ω_{IF} ranging from 41 to 45 MHz is plotted along x and amplitude in V along y axis.

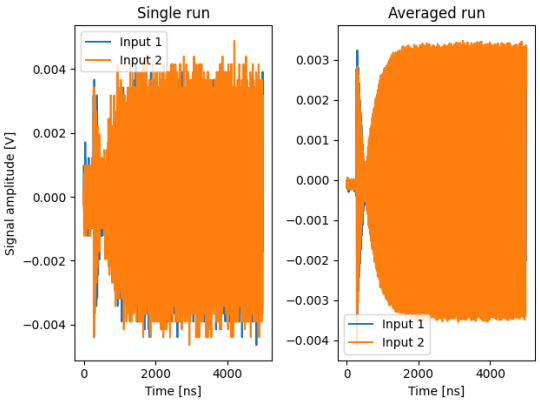

Figure 5.4: Time of flight calibration and raw ADC trace; input 1 and 2 corresponds to I and Q channel.

5.2 OPX & Octave System Calibration

The QM system was calibrated for the compensation of the time of flight and the ADC calibration as well. A readout baseband step envelop was used to calibrate the system . The prepossessed signal was analysed on the averaged run. The initial bottleneck shape(Figure5.4) is due to transient response discussed in Sec.2.3.1.

5.3 Two Tone Qubit Spectroscopy and Dispersive Readout

5.3.1 Qubit Spectroscopy(Low Power)

As discussed in Sec.4.3.2, the frequency domain measurement was carried out sweeping the qubit drive frequency and observing the cavity resonance on the cavity drive tone with qubit drive amplitude set at 25 mV. In figure(Figure5.5), plotting the qubit response with a Lorentzian

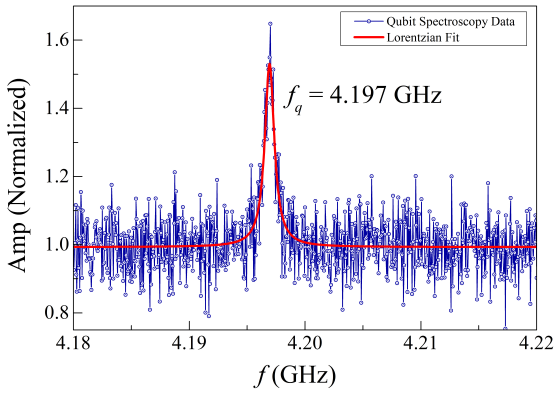

Figure 5.5: Qubit spectroscopy at low power, i.e limited photon number in the cavity to observe $|0\rangle$ to $|1\rangle$ transition of the qubit at ω_q.

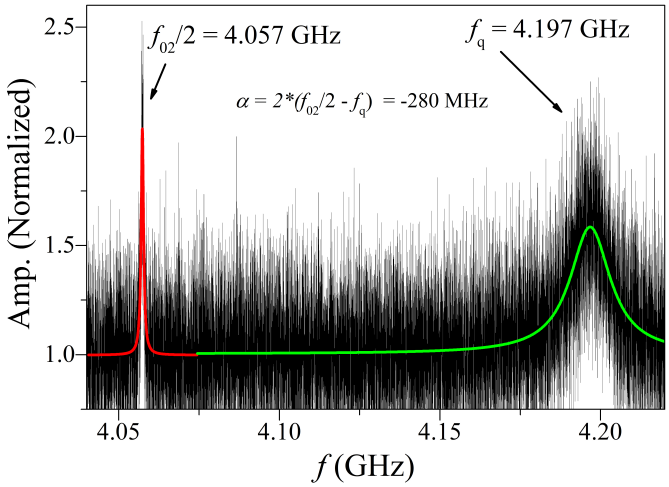

Figure 5.6: Qubit spectroscopy at high power; along with the ω_{01} transition fitted in green, $|0\rangle$ to $|2\rangle$ with two $\omega_{02}/2$ photon transition is fitted in red. Lorentzian fitting is used.

fit, the qubit transition frequency ω_q is identified to be 4.197 GHz.

5.3.2 Qubit Spectroscopy(High Power)

Upon inspecting the qubit at high power, two distinct peak was observed as expected. The sharp peak on the left corresponds to the two-photon transition process for $\omega_{02}/2$, sometimes known as the '02/2' peak. With Lorentzian fit, the data obtained from figure(Figure 5.5 & 5.6), are as followed;

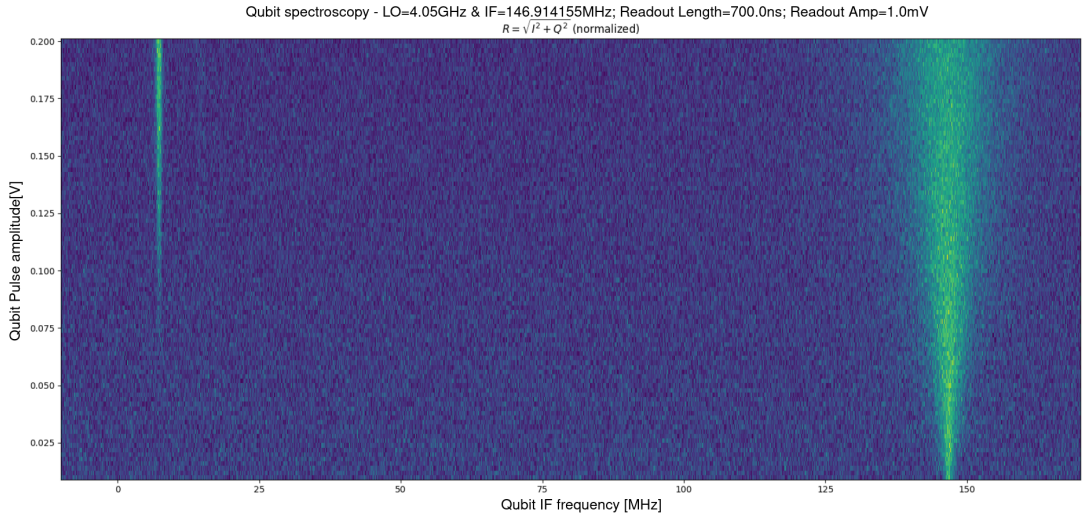

Figure 5.7: 2D plotting of qubit spectroscopy; drive pulse amplitude in V along y axis and qubit IF in MHz along x. RF frequency= LO+IF. 2-photon transition visible in the left above 75 mV of drive amplitude, and with increasing power, peak broadening in notable.

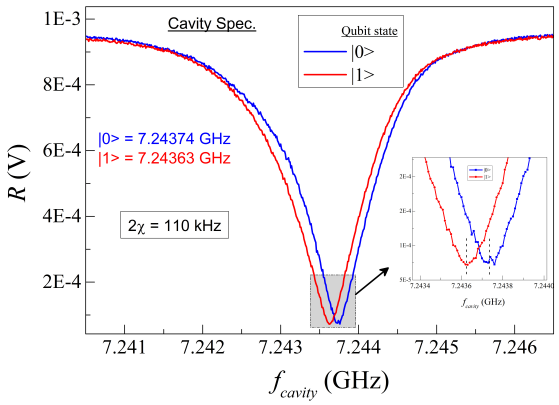

Figure 5.8: State dependency of cavity resonance frequency; Reflected signal amplitude in V is plotted along y axis against frequency in GHz on x.

- ω_q or ω_{01} is around 4.197 GHz.
- ω for two photon transition to $|2\rangle$ from $|0\rangle$, i.e. $\frac{\omega_{02}}{2}$ is 4.057 GHz.
- Anharmonicity, $\alpha = 2(\omega_{02}/2 - \omega_{01})$ is -280 MHz.

5.3.3 Dispersive Readout and χ Measurement

As discussed in Sec.1.3.1, the qubit state dependency of the cavity resonance frequency was checked and χ is calculated using two tone cavity spectroscopy(Figure5.8). This show us the qubit state change results into a deviation on the cavity frequency by an amount of $2\chi = 110$ kHz.

5.4 Time Domain Measurement

We do time-domain measurements in the same order as described in the preceding Sec.4.4. The following time domain measurements are all based on projective measurements, meaning that the qubit is either located in $|e\rangle$ or in $|g\rangle$. For each experiment below, an ensemble measurement is therefore performed, in which each data point is collected numerous times and averaged to converge to the probability that the qubit is in $|e\rangle$ or in $|g\rangle$. The qubit is left undisturbed for 1 ms($\gg T_1$) prior to each pulse sequence and subsequent measurement so that it can lose energy to the environment and relax to the ground state, which corresponds to the thermal equilibrium of $\hbar\omega \gg k_B T$.

5.4.1 Time Rabi Measurement

Using a low input power to the qubit, a Rabi experiment is the first measurement carried out. At this stage, readout power is manually adjusted to a value that will prevent the qubit from getting overwhelmed or *punched out* in order to get the best possible SNR.

The I(t) and Q(t) data streams received from the demodulation mixer are digitally turned to produce all data in Q(t). To improve visual clarity, the data is rotated by $n\pi$ so that the $|g\rangle$ has a lower Q(t) than the excited $|e\rangle$ state. We project the data on the measurement axis(z). The data is fitted to a sine curve to obtain the time length of X_π pulse.

The X_π pulse length obtained from the time Rabi oscillation is 123.2 ns.

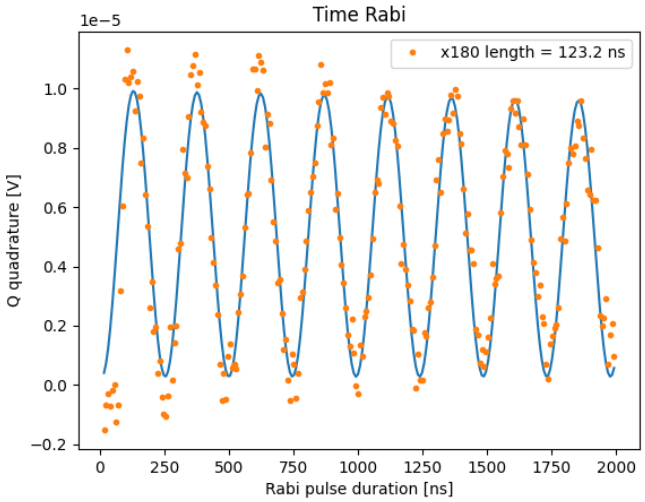

Figure 5.9: Time Rabi oscillation plot exhibiting data points in yellow fitted with a blue sine curve; and π pulse length measurement.

5.4.2 Power Rabi Measurement

In power Rabi, we calibrate the X_π pulse amplitude. The time for the pulse duration is set to be 124 ns as the clock of the OPX is 4 ns, we can not get higher time resolution than that. Now we employ pulses with varying amplitude trying to find out the optimum amplitude for the π pulse. Which in the experiment is found to be 0.101 V for the calibrated time of 124 ns.

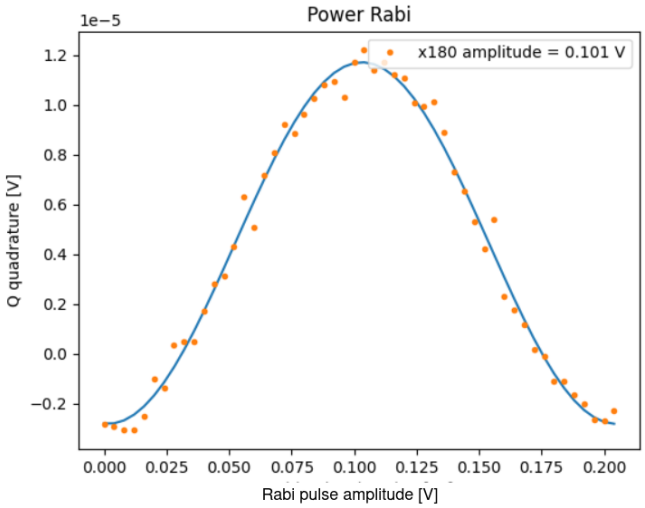

Figure 5.10: Power Rabi measurement plot exhibiting data points in yellow fitted by a blue sine curve; and π pulse amplitude calibration.

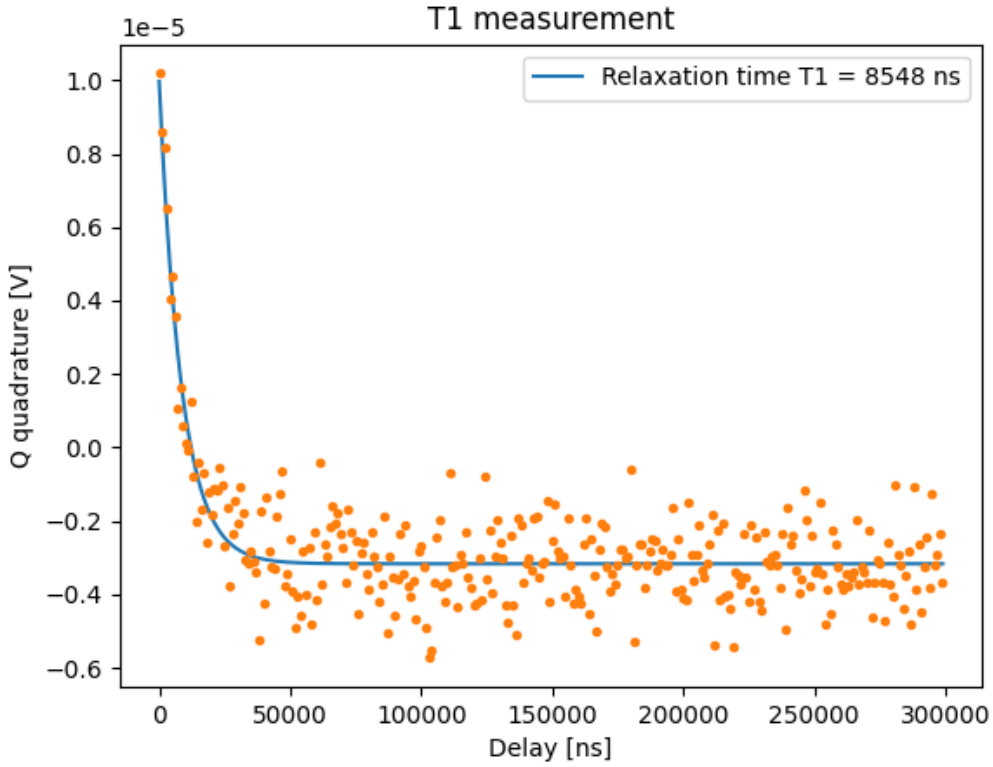

Figure 5.11: Qubit longitudinal relaxation measurement and T_1 determination; data points are in yellow and the curve fitting from E.q.(4.1) is in blue.

Although this precision is adequate for our upcoming experiments, it can yet be improved upon and will probably be required for computational manipulations. By taking stability measurements, we can achieve that.

5.4.3 Longitudinal Coherence Time T_1 Measurement

Once the π pulses and thus any transverse θ pulses are calibrated for their time length and amplitude, we are ready to perform coherence measurement. Discussed in Sec.4.4.2, T_1 is measured by letting an X_π or Y_π pulse to get the qubit in $|e\rangle$ and after gradually increasing relaxation time provided to the qubit, readout was taken for each time. From the exponential fitting of the graph, relaxation time T_1 was taken and in our experiment, it was found to be 8584 ns.

5.4.4 Ramsey Interferometry; T_2^* Measurement

Discussed in Sec.4.4.3, we perform Ramsey interferometry to obtain transverse dephasing time in order to fine tune the qubit drive frequency. We initially detune the qubit drive frequency in the order of kHZ to make the oscillation more prominent in the experiment. The detuning obtained from the fit is -86.159 kHz. The coherence time T_2^* is measured to be 1647 ns(Figure5.12). We

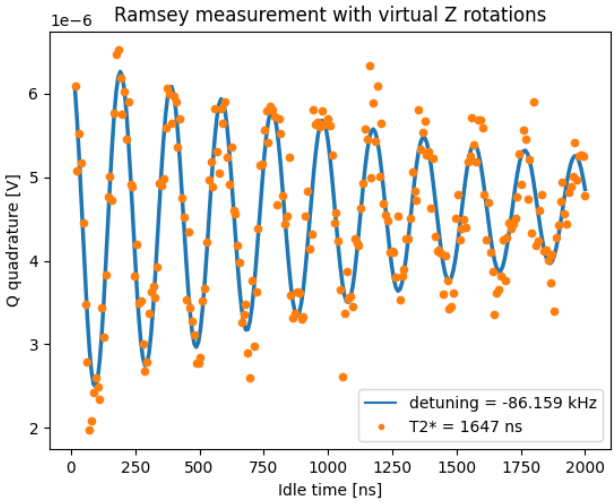

Figure 5.12: Ramsey measurement with the data points in yellow and the fit is in blue using E.q.(4.2).

can now determine the qubit frequency to within a few tens of kilohertz and proceed with the Hahn echo measurement on the qubit.

5.4.5 Hahn Echo Measurement for Coherence Time T_{2E}

The Hahn echo measurement as described in Sec.4.4.4 was performed with precise programm-ed pulse sequence. The transverse coherence time due to pure dephasing from Hahn echo experi-

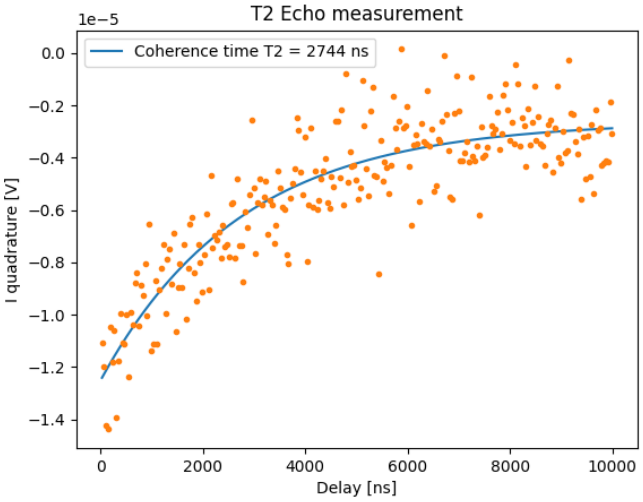

Figure 5.13: Hahn echo measurement with data points in yellow fitted in blue using E.q.(4.3).

ment(Figure5.13) is obtained to be T_{2E}=2477 ns.

5.5 Data Obtained From Characterisation Experiment

Parameter	Experiment	Obtained result
Cavity frequency	Single tone spectroscopy	7.24388 GHz
Qubit frequency	Two tone spectroscopy	4.197 GHz
Dispersive shift in Cavity frequency	Two tone spectroscopy	110 kHz
πpulse length measurement	Time Rabi oscillation	124 ns
πpulse amplitude calibration	Power Rabi measurement	0.101 V
Longitudinal coherence time T_1	T_1 measurement	8584 ns
Transverse dephasing time T_2^*	Ramsey interferometry	1647 ns
Transverse dephasing time T_{2E}	Hahn echo measurement	2477 ns

Chapter 6

Parting Remarks

The main goal of this research was to investigate a single-qubit processing unit and optimize the system along with its peripherals successfully in order to get the system ready for quantum computing. We have explored and operated a superconducting transmon qubit inside a 3D cavity. In this thesis, a "punch-out" experiment was utilized to verify the qubit's functionality first. We found the frequencies of the cavity and the qubit using frequency spectroscopy. We next stimulated the qubit over a variety of different timeframes to observe Rabi oscillations, which enabled us to calibrate the π and $\pi/2$ pulses that are the basic elements of qubit control and computational pulse programming. To account for decoherence in the system, we performed T_1 measurement, Ramsey interferometry, and Hahn echo measurement; and further calibrated the control system to optimize it for real-time qubit manipulation.

Possible improvement It is crucial to remember that the configuration we have chosen, still have room for improvement. For improved SNR, steps such as parametric amplifier in the cryogenic setup can and should be implemented. We have observed less than ideal bias reaching the HEMTs as well. Due to time constraint, I am yet to address these issues. Moving forward, there must be considerable efforts dedicated to these.

Future endeavours As the basic characterisations of the single qubit-cavity system is done and reported along with scopes of improvement in the arrangement, we should further move on in to the computational characterisations. After the issues with the system noise and decoherence are addressed properly, we have to perform stability measurement, drag pulse calibration and last but not the least, fidelity improvement of the qubit states in order to get the system computation ready.

Bibliography

[1] Richard P. Feynman. Simulating physics with computers. *International Journal of Theoretical Physics*, 21(6-7):467–488, June 1982.

[2] P. Krantz, M. Kjaergaard, F. Yan, T. P. Orlando, S. Gustavsson, and W. D. Oliver. A quantum engineer's guide to superconducting qubits. *Applied Physics Reviews*, 6(2):021318, 06 2019.

[3] Alexandre Blais, Arne L. Grimsmo, S. M. Girvin, and Andreas Wallraff. Circuit quantum electrodynamics. *Rev. Mod. Phys.*, 93:025005, May 2021.

[4] Alexandre Blais, Ren-Shou Huang, Andreas Wallraff, S. M. Girvin, and R. J. Schoelkopf. Cavity quantum electrodynamics for superconducting electrical circuits: An architecture for quantum computation. *Phys. Rev. A*, 69:062320, Jun 2004.

[5] Matthew Reagor, Wolfgang Pfaff, Christopher Axline, Reinier W. Heeres, Nissim Ofek, Katrina Sliwa, Eric Holland, Chen Wang, Jacob Blumoff, Kevin Chou, Michael J. Hatridge, Luigi Frunzio, Michel H. Devoret, Liang Jiang, and Robert J. Schoelkopf. Quantum memory with millisecond coherence in circuit qed. *Phys. Rev. B*, 94:014506, Jul 2016.

[6] E.T. Jaynes and F.W. Cummings. Comparison of quantum and semiclassical radiation theories with application to the beam maser. *Proceedings of the IEEE*, 51(1):89–109, 1963.

[7] Bruce W Shore and Peter L Knight. The Jaynes-Cummings model. *J. Mod. Opt.*, 40(7):1195–1238, July 1993.

[8] C. C. Gerry and P. L. Knight. *Introductory Quantum Optics*. Cambridge University Press, Cambridge, 2005.

[9] Maxime Boissonneault, J. M. Gambetta, and Alexandre Blais. Dispersive regime of circuit qed: Photon-dependent qubit dephasing and relaxation rates. *Phys. Rev. A*, 79:013819, Jan 2009.

[10] Alexandre Blais, Jay Gambetta, A. Wallraff, D. I. Schuster, S. M. Girvin, M. H. Devoret, and R. J. Schoelkopf. Quantum-information processing with circuit quantum electrodynamics. *Phys. Rev. A*, 75:032329, Mar 2007.

[11] Mahdi Naghiloo. Introduction to experimental quantum measurement with superconducting qubits, 2019.

[12] David M. Pozar. *Microwave Engineering*. John Wiley & Sons, Inc., USA, 2011.

[13] Li Tan and Jean Jiang. *Digital signal processing: fundamentals and applications*. Academic press, 2018.

[14] Anthony E Siegman. *Lasers*. University science books, 1986.

[15] D. M. Berns, W. D. Oliver, S. O. Valenzuela, A. V. Shytov, K. K. Berggren, L. S. Levitov, and T. P. Orlando. Coherent quasiclassical dynamics of a persistent current qubit. *Phys. Rev. Lett.*, 97:150502, Oct 2006.

[16] Misha Turlakov. Johnson-nyquist noise in films and narrow wires. *Phys. Rev. B*, 62:4656–4660, Aug 2000.

[17] I. Siddiqi, R. Vijay, F. Pierre, C. M. Wilson, M. Metcalfe, C. Rigetti, L. Frunzio, and M. H. Devoret. Rf-driven josephson bifurcation amplifier for quantum measurement. *Phys. Rev. Lett.*, 93:207002, Nov 2004.

[18] Ananda Roy and Michel Devoret. Quantum-limited parametric amplification with josephson circuits in the regime of pump depletion. *Phys. Rev. B*, 98:045405, Jul 2018.

[19] R Vijay, M Devoret, and I Siddiqi. Invited review article: The josephson bifurcation amplifier. *The Review of scientific instruments*, 80:111101, 11 2009.

[20] Olli Mansikkamäki, Alexander Tyner, Alexander Bilmes, Ilya Drozdov, and Alexander Balatsky. Two-tone spectroscopy for the detection of two-level systems in superconducting qubits, 2024.

[21] R. Merlin. Rabi oscillations, Floquet states, Fermi's golden rule, and all that: Insights from an exactly solvable two-level model. *American Journal of Physics*, 89(1):26–34, 01 2021.